

The neutral gas content of post-merger galaxies.

Sara L. Ellison¹, Derek Fertig², Jessica L. Rosenberg², Preethi Nair³, Luc Simard⁴, Paul Torrey⁵, David R. Patton⁶

¹ *Department of Physics & Astronomy, University of Victoria, Finnerty Road, Victoria, British Columbia, V8P 1A1, Canada.*

² *School of Physics, Astronomy, and Computational Science, George Mason University, MS 3F3, 4400 University Drive, Fairfax, VA 22030, USA.*

³ *Dept. of Physics & Astronomy, University of Alabama, 514 University Blvd, Tuscaloosa, Alabama, 35487, USA*

⁴ *National Research Council of Canada, 5071 West Saanich Road, Victoria, BC V9E 2E7, Canada*

⁵ *Harvard Smithsonian Center for Astrophysics, 60 Garden Street, Cambridge, MA 02138, USA*

⁶ *Department of Physics & Astronomy, Trent University, 1600 West Bank Drive, Peterborough, Ontario, K9J 7B8, Canada.*

14 January 2015

ABSTRACT

Measurements of the neutral hydrogen gas content of a sample of 93 post-merger galaxies are presented, from a combination of matches to the ALFALFA.40 data release and new Arecibo observations. By imposing completeness thresholds identical to that of the ALFALFA survey, and by compiling a mass-, redshift- and environment-matched control sample from the public ALFALFA.40 data release, we calculate gas fraction offsets (Δf_{gas}) for the post-mergers, relative to the control sample. We find that the post-mergers have HI gas fractions that are consistent with undisturbed galaxies. However, due to the relative gas richness of the ALFALFA.40 sample, from which we draw our control sample, our measurements of gas fraction enhancements are likely to be conservative lower limits. Combined with comparable gas fraction measurements by Fertig et al. in a sample of galaxy pairs, who also determine gas fraction offsets consistent with zero, we conclude that there is no evidence for significant neutral gas consumption throughout the merger sequence. From a suite of 75 binary merger simulations we confirm that star formation is expected to decrease the post-merger gas fraction by only 0.06 dex, even several Gyr after the merger. Moreover, in addition to the lack of evidence for gas consumption from gas fraction offsets, the observed HI detection fraction in the complete sample of post-mergers is twice as high as the controls, which suggests that the post-merger gas fractions may actually be enhanced. We demonstrate that a gas fraction enhancement in post-mergers, relative to a stellar mass-matched control sample, would indeed be the natural result of merging randomly drawn pairs from a parent population which exhibits a declining gas fraction with increasing stellar mass.

Key words: Galaxies: interactions, galaxies: ISM, galaxies: peculiar

1 INTRODUCTION

Galaxies require gas for star formation. There exist several ways in which this gas can be acquired, such as feeding through intergalactic filaments, accretion of satellites and major mergers (e.g. Keres et al. 2005; Wang et al. 2011; L’Huillier, Combes & Semelin 2012; and see Sancisi et al. 2008 and Sanchez Almeida et al. 2014 for reviews). There is compelling evidence that the gas reservoir must be continually replenished if star formation is to continue (see Putman, Peek & Joing 2012 for a review and discussion of various refuelling mechanisms). For example, whilst the total stellar mass of galaxies on the red sequence increases signifi-

cantly towards lower redshifts, both the mass in galaxies in the ‘blue cloud’ (Bell et al. 2004, 2007; Borch et al. 2006; Faber et al. 2007) and the mass density of HI in high column density QSO absorbers (e.g. Guimaraes et al. 2009; Noterdaeme et al. 2012; Zafar et al. 2013) exhibit no strong evolution with redshift. This lack of evolution contrasts with the star formation rate (SFR) density, which evolves strongly over the epochs probed by these observations (e.g. Lilly et al. 1996; Madau et al. 1998; Hopkins & Beacom 2006). Refuelling of the galactic gas reservoir seems inevitable and is both widely predicted by simulations and supported by observations (e.g. Keres et al. 2005; Oosterloo et al. 2007a; Sancisi et al. 2008; Brooks et al. 2009).

Galaxy mergers provide a natural way to deliver a fresh supply of gas to galaxies (although perhaps not sufficient to maintain current rates of star formation, e.g. Di Teodoro & Fraternali 2014). This delivery mechanism usually triggers new episodes of star formation in both the pre-coalescence phase (Barton, Geller & Kenyon 2000; Nikolic, Cullen & Alexander 2004; Alonso et al. 2006; Woods, Geller & Barton 2006; Ellison et al. 2008a, 2013b; Li et al. 2008; Scudder et al. 2012; Patton et al. 2013) and the final merger remnant (Wang et al. 2006; Kartelstepe et al. 2010; Daddi et al. 2010a; Genzel et al. 2010; Carpineti et al. 2012; Kaviraj et al. 2012; Shabala et al. 2012; Ellison et al. 2013a; Kaviraj 2014). Such bursts of star formation may plausibly lead to a more rapid depletion of the gas reservoir. However, observational results on this topic have yielded mixed results. Braine & Combes (1993) found the HI content of disturbed galaxies to be similar to that of unperturbed galaxies, and concluded that the HI content was unaffected by interactions. In contrast, observations of HI in post-starburst galaxies, which are implicated as merger-driven (Zabludoff et al. 1996; Blake et al. 2004), find HI gas fractions that are low relative to late-types (presumably the merger progenitors) of the same stellar mass (Zwaan et al. 2013). However, compared to early types, the post-starbursts are relatively HI rich (Zwaan et al. 2013).

In addition to supplying fresh gas, the merger may also re-distribute the gas, potentially making it unavailable for sustained star formation. For example, maps of HI in nearby galaxy pairs and post-mergers reveal long tidal gas tails and bridges that can extend up to a few hundred kpc (Hibbard & Yun 1999; Wang et al. 2001; Koribalski & Dickey 2004). Gas-rich ellipticals, which may be merger remnants, sometimes exhibit large HI masses distributed in extended structures, but with surface densities that are insufficient to form new stars (Oosterloo et al. 2007b). Indeed, it has been suggested that the long lifetimes of such extended HI structures, which may have no (or very low surface brightness) optical counterparts (Hibbard & Yun 1999; Buyle et al. 2008) may be an effective way of identifying mergers long after optical disturbances have faded (Hibbard & van Gorkom 1996; Holwerda et al. 2011; Lelli, Verheijen & Fraternali 2014).

Despite these numerous individual studies, larger samples, coupled with a comparison to isolated (i.e. non-merger) galaxies of similar properties, are required to form a statistical picture of the evolution of gas content during the merger sequence. In Fertig et al. (2015) we investigated the evolution of HI gas fractions in the pre-merger phase of a sample of close galaxy pairs. Despite well documented SFR enhancements in this same sample (Scudder et al. 2012; Patton et al. 2013), Fertig et al. (2015) do not detect any decline in the HI gas fraction of close pairs. Indeed, in an earlier study based on a small sample of confusion-free HI measurements, Huchtmeier et al. (2008) suggested that mergers may be relatively HI-rich. Casasola et al. (2004) present a similar study, but with over 1000 galaxies drawn from all interaction stages, from well separated pairs to coalesced remnants. HI gas fractions are again found to be enhanced by a factor of ~ 10 in early type systems, but much more modestly over-abundant in late type galaxies.

There are a few possible reasons why previous studies have not detected depletion in merger gas fractions. First, in order to obtain a complete view of gas depletion, it is impor-

tant to consider both atomic and molecular gas, the latter of which may be expected to be more closely linked to star formation. One of the first studies of the combined atomic and molecular content of galaxy mergers was performed by Braine & Combes (1993), in which it was found that the molecular gas fraction is enhanced in interacting galaxies. Bettoni et al. (2001), from a study of the CO and HI content of polar ring galaxies (which have likely formed through a past merger), also found gas fractions that are enhanced by an order of magnitude. Enhanced molecular gas fractions soon after a merger are predicted by simulations (Bekki 2014), although eventually the gas is consumed by the triggered star formation. Stark et al. (2013) measured elevated molecular fractions in galaxies selected to have anomalously blue centres, which are frequently the signature of a recent merger. A similar result is found by Goncalves et al. (2014) who measure elevated CO fractions in their local sample of Lyman Break Analogs, many of which show merger properties. Ultra-luminous infra-red galaxies (ULIRGs), which are often merger driven, also manifest very high CO gas fractions (Daddi et al. 2010b). Most recently, Ueda et al. (2014) have used a sample of 37 post-mergers to show that molecular gas disks are a common feature of merger remnants, indicating that these reservoirs have not yet been exhausted by merger driven star formation.

A second potential reason for the lack of HI depletion in mergers is the relatively small consumption expected in the pre-merger (pairs) phase. Fertig et al. (2015) used a suite of binary merger simulations to show that, even at the closest separations, the HI gas mass is expected to be depleted by only ~ 0.04 dex. This is a relatively small effect that can be challenging to detect in small samples. Signatures of gas depletion may be more obvious in late-stage mergers, where simulations predict that SFRs will peak (e.g. Mihos & Hernquist 1996; Di Matteo et al. 2007, 2008; Montuori et al. 2010; Torrey et al. 2012). In Ellison et al. (2013a) we confirmed the prediction of high SFRs by combining a sample of galaxy pairs (with separations up to 80 kpc) and post-mergers. There is a steady increase in the SFR enhancements with decreasing separation, peaking in the post-mergers. We may therefore expect that the most rapid consumption of gas occurs after coalescence, depending on the rate of star formation and its duration. Indeed, simulations of galactic gas reservoirs of both atomic and molecular gas show an increase in gas fraction before a decline at later times (Bekki 2014; Rafieeantsoa et al. 2014). The initial increase in HI gas fraction may be linked to the condensation of hot halo gas into the disk (Moster et al. 2011; Tonnesen & Cen 2012). High molecular gas fractions may follow from the increased central surface densities that precede starbursts in mergers. Indeed, several previous observational studies have measured increased gas fractions in either atomic or molecular gas (Braine & Combes 1993; Bettoni et al. 2001; Huchtmeier et al. 2008; Stark et al. 2013; Goncalves et al. 2014).

In this paper, we present a systematic study of HI masses in a moderately large sample of 93 recently merged galaxies. The sample is constructed from both new Arecibo observations, combined with publicly available HI masses measured as part of the Arecibo Legacy Fast ALFA (ALFALFA) project (Giovanelli 2005a,b; Saintonge 2007). Through a careful matching of the post-mergers with a sample of isolated (non-merger) galaxies, it is possible to quan-

tify the enhancement or deficit in gas fraction associated with the merger process. Finally, we interpret our results with the aid of hydrodynamical merger simulations.

We adopt a cosmology of $\Omega_\Lambda = 0.7$, $\Omega_M = 0.3$, $H_0 = 70$ km/s/Mpc.

2 SAMPLES AND OBSERVATIONS

2.1 The Ellison et al. (2013a) Galaxy Zoo post-merger sample

Ellison et al. (2013a) identified and studied the optical properties of 97 post-merger galaxies, selected from the SDSS, based on the visual classifications of the Galaxy Zoo project (Darg et al. 2010). In brief, the Galaxy Zoo visual identifications are performed on some 900,000 galaxies in the SDSS DR6, as described in Lintott et al. (2008). For the compilation of their merger samples, Darg et al. (2010) additionally required $0.0005 < z < 0.1$ and $m_r < 17.77$. Further visual classification was performed by Ellison et al. (2013a) with the additional requirements that galaxies have an SDSS specclass=2 and that a Mendel et al. (2014) stellar mass must be available. The final sample is characterized by single late stage mergers that are highly disturbed (i.e. these are not galaxy pairs), with distinctive shells and tidal features and is therefore likely to be dominated by the remnants of gas-rich major mergers. Although it is not possible to know the exact mass ratio of the mergers that formed these remnants, simulations indicate that the mass ratios were likely closer than 1:4 (e.g. Lotz et al. 2010b; Ji, Peirani & Yi 2014).

2.1.1 Matches with ALFALFA.40

The Ellison et al. (2013a) post-merger sample was cross-correlated with the ALFALFA survey (Giovanelli et al. 2005a,b). ALFALFA is a large survey conducted with the Arecibo telescope covering ~ 7000 square degrees of sky, with a frequency coverage between 1335 and 1435 MHz, i.e. with coverage of the 21 cm line extending to $z \sim 0.06$. The survey is conducted in a drift scan mode, such that sensitivity is naturally dependent on the galaxy distance. Giovanelli et al. (2005a) estimate the HI mass limit to be $\sim 10^6 M_\odot$ at a distance of 6.5 Mpc and $10^7 M_\odot$ at 20 Mpc. The 40% data release (ALFALFA.40, Haynes et al. 2011) covers ~ 2800 square degrees and contains $\sim 15,000$ extragalactic sources. For the cross-matching, we searched for ALFALFA.40 detections within a 1.5 arcmin radius and a difference in recessional velocity of less than 500 km/s for each post-merger. In practice, most matches were successfully made with offsets < 30 arcseconds. This procedure yielded 8 matches, see Table 1. Of these 8, 7 are flagged as high quality detections in ALFALFA.40 (identified by the survey as code 1). In addition, there is one SDSS post-merger (objID=587736808845082795) that is associated with an ALFALFA.40 source that is flagged as a code 2 galaxy¹.

¹ The ALFALFA catalog allocates a code 2 flag for galaxies with detections whose $S/N < 6.5$. or with otherwise noisy spectra. In the case of objID=587736808845082795, the data cube is significantly affected by RFI, hence the classification as ‘code 2’, despite the relatively high formal S/N .

For one object, objID=587736479206342888, the ALFALFA.40 catalog reports a suspiciously low velocity width of 27 km s^{-1} . Upon inspection of the spectrum, the data were found to be very noisy with a possible second component in the emission. The original spectrum only measured one narrow peak resulting in a under estimate of the velocity width. We applied further smoothing to the spectrum and re-measured the flux adding the second peak. From this spectrum we then re-computed the parameters for this galaxy with our own data reduction tools, and report the final adopted value in Table 1.

2.1.2 Targeted Arecibo observations

A further 37 post-mergers were observed during two runs (PI Fertig) with the Arecibo telescope on August 19 and December 28, 29 2013, see Table 2. The observations used the L-band wide receiver with the Interim Correlator and 9-level sampling with 2 polarizations per board. As for the ALFALFA survey, we used the WAPP spectrometers with a total bandwidth of 100MHz centered on 1385 Mhz. The observations were designed to reach a 5σ HI mass limit of 10% of the stellar mass. The minimum exposure time for the ON+OFF was set to be 4 minutes. For four of the sources the observing time was capped at 30 minutes, yielding a 5σ HI mass limit of 50% of the stellar mass or better. For the data reduction, the spectra were Hanning smoothed and then reduced using standard ON-OFF reduction. Five sources were observed on 19 August – two were detections and three were non-detections. An additional 32 sources were observed on 28 and 29 December resulting in 10 more detections. Reduced spectra of the 12 new detections are shown in Fig. 1. The final resolution ranges between 10 and 14 km s^{-1} , depending on smoothing.

Table 2 lists various target and observational parameters, including exposure times, fluxes and the final derived HI masses for our Arecibo observations. HI masses (in units of solar masses) are calculated using the following formula:

$$M(\text{HI}) = 2.356 \times 10^5 \times D^2 S_{21} \quad (1)$$

where D is the distance to the source in Mpc (cz/H_0 , consistent with ALFALFA) and S_{21} is the 21 cm line flux in Jy km s^{-1} . All detections have $S/N > 5$, with 11/37 of the spectra having $S/N > 6.5$ (the requirement for a code 1 classification in the ALFALFA.40 catalog). The limiting flux for non-detections is calculated from

$$S_{21} = S/N \times \frac{\text{RMS } W_{50}}{w_{sm}^{0.5} 1000} \quad (2)$$

where the RMS is measured from the spectrum and w_{sm} is a smoothing width. This latter parameter is either $W_{50}/20$ for $W_{50} < 400 \text{ km/s}$ or $400/20=20$ for $W_{50} > 400 \text{ km/s}$. For non-detections, the full width at half maximum (FWHM) line width W_{50} is calculated from the i -band Tully Fisher relation (Giovanelli et al. 1997). The 21 cm flux limits for the non-detections were then calculated from the inferred W_{50} values inserted into equation 2 for a limiting S/N (significance) of 6.5 in order to be consistent with values quoted from ALFALFA. The non-detections in Table 1 therefore have the S/N fixed to a value of 6.5.

Table 1. HI masses from the ALFALFA.40 sample matched to post-mergers in the Ellison et al. (2013a) Galaxy Zoo sample.

SDSS objid	AGC #	R.A.	dec.	redshift	$\log M_\star$ (M_\odot)	W_{50} (km s^{-1})	S_{21} (Jy km s^{-1})	RMS (mJy)	S/N	$\log M(\text{HI})$ (M_\odot)
588010880366477449	212593	172.62860	5.8920	0.03493	10.26	279 ± 27	1.86 ± 0.12	2.51	9.90	10.02 ± 0.03
587736479206342888	714739	228.22300	10.1099	0.03740	8.90	133 ± 9	0.83 ± 0.13	2.10	8.60	9.70 ± 0.07
587739132428157191	727297	237.06779	25.5270	0.04173	10.06	271 ± 40	1.19 ± 0.10	2.34	6.90	9.96 ± 0.04
587736543096799321	253937	226.32449	8.1540	0.03912	10.01	151 ± 31	0.96 ± 0.07	2.24	7.80	9.82 ± 0.03
587724233182412906	113181	28.62170	14.1960	0.05065	9.64	98 ± 36	1.35 ± 0.06	2.33	12.90	10.16 ± 0.02
587739382067822837	727193	234.00630	25.5510	0.03616	10.44	319 ± 19	1.33 ± 0.10	2.35	7.10	9.88 ± 0.03
587736808845082795	245068	223.05690	12.0609	0.05250	10.48	291 ± 7	2.01 ± 0.09	2.16	12.20	10.39 ± 0.02
588010880378404942	8372	199.99110	5.8080	0.02134	10.51	346 ± 10	2.89 ± 0.10	2.23	15.50	9.79 ± 0.01

The AGC number refers to the ALFALFA catalog number. W_{50} is the FWHM of the 21 cm emission line, S_{21} is the integrated 21 cm line flux. Derivations of the RMS and S/N are given in Haynes et al. (2011). Stellar masses are taken from the single Sérsic fits of Mendel et al. (2014). For objID=587736479206342888 the spectral parameters (including W_{50} , S_{21} , the RMS and final derived HI mass) are determined from our own re-analysis of the ALFALFA data.

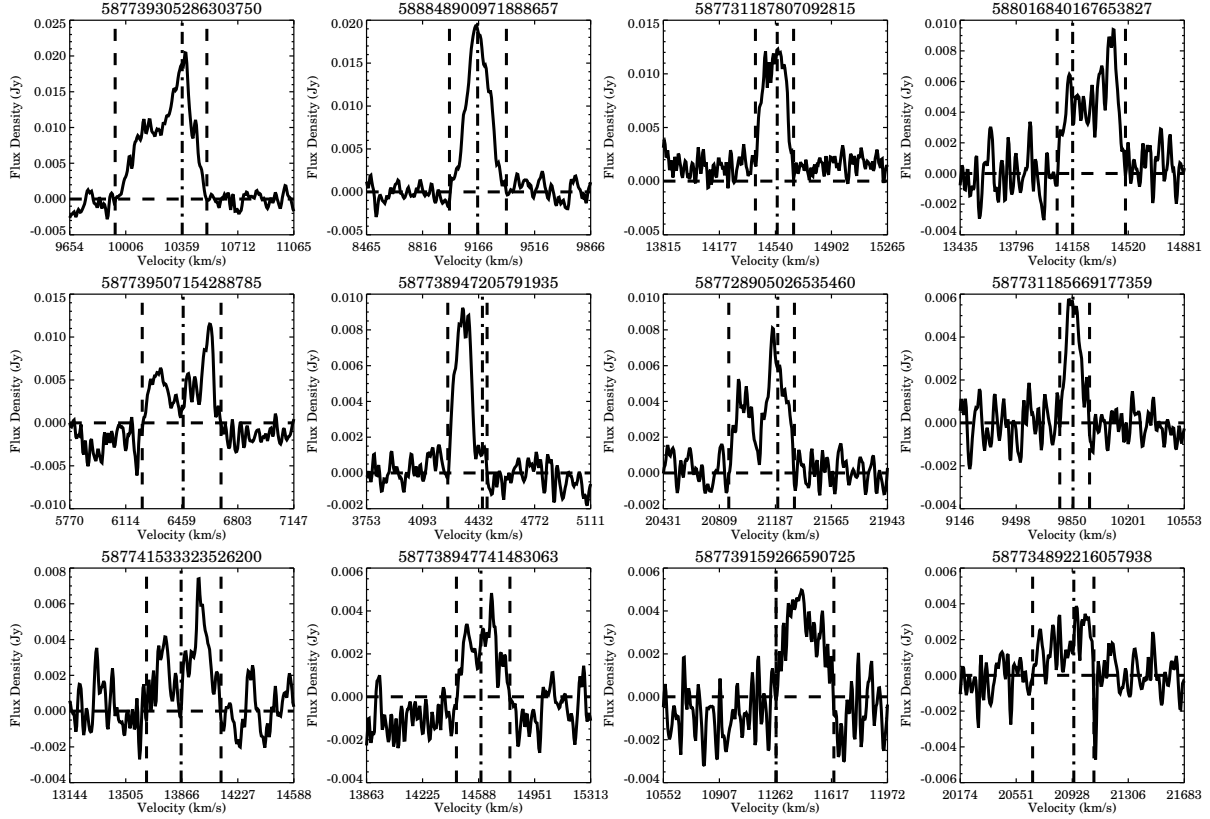


Figure 1. Spectra of the 21 cm emission lines for the 12 new detections in our post-merger sample (see Table 2). The vertical dashed lines indicate the velocity range over which the flux is summed and the vertical dot-dash line shows the redshift derived from the optical spectrum. The SDSS objID is given above each panel.

Combined with the ALFALFA.40 matches, we therefore have a total of 45 HI mass measurements for the Ellison et al. (2013a) Galaxy Zoo post-merger sample, of which 20 are detections and 25 are upper limits.

2.2 The Nair & Abraham (2010) supplementary sample.

In order to expand our post-merger sample, we used the visual classifications of $\sim 14,000$ galaxies from Nair & Abraham (2010). The Nair & Abraham classifications are also based on SDSS images, but from the DR4 and with slightly different magnitude and redshift thresholds from those of

Table 2. Target list and parameters for Aug. and Dec 2013 Arecibo observations.

SDSS objid	R.A.	dec.	redshift	log M_* (M_\odot)	Time (ON+OFF)	W_{50} (km s $^{-1}$)	S_{21} (Jy km s $^{-1}$)	RMS (mJy)	S/N	log M(HI) (M_\odot)
587731187807092815	343.01901	1.2500	0.04854	10.10	1140	190 \pm 10	2.23 \pm 0.29	2.33	15.62	10.35 \pm 0.06
587731185669177359	4.87780	-0.6020	0.03287	9.32	1800	100 \pm 8	0.57 \pm 0.07	0.89	14.14	9.42 \pm 0.05
588016840167653827	117.37570	18.9580	0.04724	10.37	240	351 \pm 16	2.08 \pm 0.27	1.82	13.71	10.31 \pm 0.06
587728905026535460	119.24500	34.0929	0.07073	10.05	1200	342 \pm 12	1.62 \pm 0.15	1.02	19.12	10.54 \pm 0.04
587738947741483063	140.58290	31.2859	0.04871	9.72	1800	227 \pm 15	0.74 \pm 0.15	1.20	9.08	9.88 \pm 0.09
587738947205791935	143.69679	32.1430	0.01486	8.52	1800	122 \pm 6	1.07 \pm 0.10	0.95	22.87	8.99 \pm 0.04
588848900971888657	146.79910	0.7030	0.03055	9.44	1200	170 \pm 9	3.20 \pm 0.27	2.07	26.49	10.11 \pm 0.04
587739159266590725	153.54409	34.3429	0.03758	9.99	240	189 \pm 26	1.08 \pm 0.15	1.08	16.23	9.83 \pm 0.06
587739305286303750	172.32220	35.5769	0.03457	10.96	360	369 \pm 15	5.29 \pm 0.42	2.66	23.15	10.43 \pm 0.03
587741533323526200	173.78129	29.8910	0.04624	11.07	240	333 \pm 10	1.25 \pm 0.16	1.25	12.24	10.06 \pm 0.06
587739507154288785	185.06550	33.6609	0.02157	10.46	240	414 \pm 6	2.06 \pm 0.26	1.98	11.18	9.62 \pm 0.05
587734892216057938	179.54049	9.5360	0.06985	10.69	240	147 \pm 25	0.71 \pm 0.12	2.31	5.66	10.17 \pm 0.07
588015510343712908	20.46209	0.8470	0.09898	11.15	240	438	<0.91	1.43	6.5	<10.59
587730775492001995	342.48558	14.8750	0.08993	10.69	540	320	<0.42	0.81	6.5	<10.17
587731185651810753	325.23431	-0.4780	0.06816	9.74	1800	185	<0.51	1.28	6.5	<10.01
587738372206690585	120.58889	19.9939	0.06771	10.58	240	359	<0.91	1.65	6.5	<10.26
587732470387703859	129.57679	33.5779	0.06212	11.18	240	470	<1.45	2.13	6.5	<10.38
587732484342415393	130.93750	35.8279	0.05393	11.04	240	373	<0.99	1.75	6.5	<10.09
587744729564512606	133.78070	15.2690	0.07681	10.99	240	523	<1.07	1.41	6.5	<10.44
587738409785557168	143.44760	10.8120	0.08558	11.33	240	369	<0.77	1.38	6.5	<10.39
587735349633351728	148.30130	13.1009	0.07709	11.34	240	374	<0.83	1.47	6.5	<10.33
587738947747053602	154.64019	36.2239	0.05412	10.95	240	439	<1.49	2.33	6.5	<10.27
587726032776265859	159.13279	2.3620	0.05026	10.30	240	279	<1.15	2.36	6.5	<10.10
587734948595236905	160.26559	11.0959	0.05297	10.82	240	434	<0.83	1.32	6.5	<10.00
587732702329045015	160.29069	6.8200	0.03332	10.57	240	344	<0.88	1.63	6.5	< 9.63
588848900441112762	160.79060	0.3140	0.09788	11.01	240	590	<1.77	2.07	6.5	<10.87
588017702386270301	162.93029	10.7570	0.09734	11.52	240	448	<0.83	1.28	6.5	<10.53
588017703997276265	163.71000	12.0900	0.08045	10.55	480	244	<0.53	1.17	6.5	<10.17
588848900981260449	168.23460	0.7260	0.09687	11.24	240	348	<0.94	1.73	6.5	<10.58
587741533859414124	171.14239	30.0960	0.05492	10.74	240	257	<0.71	1.53	6.5	< 9.97
587742013816897595	175.26300	22.0480	0.06290	9.91	960	297	<0.65	1.30	6.5	<10.05
587742062680015040	176.18339	23.1620	0.04839	10.58	240	415	<0.95	1.57	6.5	< 9.98
587742062680997918	178.51669	23.3400	0.05093	10.16	240	426	<0.80	1.29	6.5	< 9.95
587726031175221368	180.99819	1.4110	0.02230	10.18	240	205	<0.58	1.39	6.5	< 9.10
588017703469777068	185.68820	12.2939	0.09209	11.54	240	568	<1.62	1.96	6.5	<10.77
588017730842853516	201.19819	8.2950	0.05179	10.94	240	293	<0.85	1.70	6.5	< 9.99
587741603112157297	201.27389	27.5450	0.07209	10.85	240	405	<0.94	1.59	6.5	<10.32

The AGC number refers to the ALFALFA catalog number. W_{50} is the FWHM of the 21 cm emission line for detections and calculated from the i -band Tully Fisher relation for non-detections (Giovanelli et al. 1997). S_{21} is the integrated 21 cm line flux. Derivations of the RMS and S/N are given in Haynes et al. (2011). The S/N is set to 6.5 for all non-detections. Stellar masses are taken from the single Sersic fits of Mendel et al. (2014).

Galaxy Zoo: $m_g < 16$ and $0.01 < z < 0.1$. However, although the Nair & Abraham catalog is largely a subset of the much larger Galaxy Zoo sample, complementary classifications exist, due to the different approaches taken by classifiers (the statistical output of non-expert crowd-sourcing vs. a single expert eye). In particular, the Galaxy Zoo classifications are biased towards the most highly disturbed mergers, which are obvious from a brief inspection of the SDSS postage stamp images provided to the public. Conversely, the Nair & Abraham (2010) catalog additionally identifies more subtle, and often low surface brightness, features such as faint shells and tidal tails, as we demonstrate below.

We compile the supplementary sample of post-mergers in two steps. First, we make use of 411 potential late-stage post-mergers, galaxies with strong shells and tidal features

and close companions with merger classifications not present in the original Nair & Abraham (2010) catalog. We supplement this with a query of the published catalog to identify galaxies with an `interaction_flag` > 2 , but with the `pair_flag` $= 0$, which yields 77 galaxies. These lists are not unique. Both lists are cross-matched with ALFALFA.40, combined, and then duplicates between the two, and with the Ellison et al. (2013a) sample, are excluded. The final Nair & Abraham post-merger sample contains 48 galaxies with ALFALFA matches, of which 23 have detections and 25 have upper limits (Table 3). As for our targeted Arecibo sample, we list the FWHM (W_{50}) of the 21 cm emission line for detections and the width derived from the i -band Tully-Fisher for non-detections, as described in the previous section. Derivations of the RMS and S/N are given in Haynes et

Table 3. HI masses from the ALFALFA.40 sample matched to post-mergers selected from Nair & Abraham (2010)

SDSS objid	AGC #	R.A.	dec.	redshift	$\log M_\star$ (M_\odot)	W_{50} (km s^{-1})	S_{21} (Jy km s^{-1})	RMS (mJy)	S/N	$\log M(\text{HI})$ (M_\odot)
587724232100282512	100318	8.77704	14.3548	0.03801	10.02	299±22	2.23±0.10	2.37	12.1	10.12±0.02
587724232641937419	110216	20.011	14.3618	0.03104	10.12	83±13	1.13±0.06	1.94	14.2	9.66±0.02
587724233720332316	...	30.9965	14.3104	0.04269	10.92	384	<1.28	2.25	6.5	<10.00
587726101750546619	231606	210.551	4.58573	0.04031	11.02	421±27	1.68±0.12	2.44	7.3	10.09±0.03
587727221949530261	...	357.996	14.7511	0.04668	10.95	408	<1.33	2.25	6.5	<10.10
587727223020454084	...	351.309	15.2448	0.04342	10.40	276	<1.09	2.25	6.5	< 9.95
587728880873701381	...	146.112	4.49914	0.04671	10.58	408	<1.33	2.25	6.5	<10.10
587728881413390384	201303	152.655	5.15067	0.01367	9.10	134±9	1.41±0.07	2.32	11.7	9.11±0.02
587728881418502205	6049	164.38	5.69873	0.05320	11.16	290±3	1.98±0.11	2.56	10.1	10.41±0.02
587729158966345769	222264	194.588	4.88565	0.03612	10.22	355±10	1.68±0.13	2.67	7.5	10.00±0.03
587729160042119249	...	199.249	5.65679	0.03306	10.77	343	<1.21	2.25	6.5	< 9.76
587730774424223763	...	356.624	14.8867	0.05751	10.77	330	<1.19	2.25	6.5	<10.23
587732053235794407	...	118.396	26.4624	0.03645	10.18	190	<0.90	2.25	6.5	< 9.72
587732577233469472	...	154.101	5.6954	0.04899	10.97	325	<1.18	2.25	6.5	<10.09
587732577774469219	201673	163.518	6.72539	0.02659	10.38	229±3	1.96±0.08	2.12	13.6	9.81±0.02
587732578837201105	191115	138.302	5.61087	0.05846	10.99	206±7	1.30±0.10	2.71	7.4	10.30±0.03
587732579385933949	213056	165.496	8.10891	0.03019	9.76	219±12	1.78±0.09	2.32	11.6	9.88±0.02
587732702331535424	...	166.047	7.06904	0.03255	10.71	274	<1.08	2.25	6.5	< 9.70
587732702868865044	...	167.004	7.44229	0.04111	10.62	374	<1.27	2.25	6.5	< 9.97
587732703398527109	...	150.393	6.93203	0.04892	11.31	428	<1.40	2.25	6.5	<10.16
587732771053830198	...	178.604	9.60905	0.03517	10.55	329	<1.19	2.25	6.5	< 9.80
587732771053830214	210905	178.637	9.54455	0.03576	9.70	180±11	1.06±0.09	2.53	7.0	9.80±0.03
587732772126785620	210781	176.792	10.5177	0.02137	9.57	100±9	0.55±0.06	2.21	5.5	9.08±0.04
587732772130652231	...	185.741	10.5483	0.02594	10.54	304	<1.14	2.25	6.5	< 9.52
587734622163763258	180008	120.867	25.1027	0.02758	10.08	237±74	0.96±0.09	2.39	5.8	9.52±0.04
587734891683119143	220805	188.681	9.00471	0.04306	10.67	286±65	0.84±0.10	2.44	4.5	9.85±0.05
587734892216713241	...	181.066	9.3969	0.03525	10.64	354	<1.23	2.25	6.5	< 9.82
587734893287440431	210497	174.042	10.0556	0.02073	10.41	261±23	2.87±0.11	2.32	17.1	9.77±0.02
587734894357446674	...	165.312	10.4811	0.04222	10.84	346	<1.22	2.25	6.5	< 9.97
587734948054696027	...	151.83	9.87247	0.05735	11.17	452	<1.48	2.25	6.5	<10.32
587735347489341442	202805	156.547	12.5738	0.03096	10.14	292±14	1.77±0.10	2.34	9.9	9.90±0.02
587735348021624886	...	145.944	11.4564	0.03906	10.75	270	<1.08	2.25	6.5	< 9.85
587735348025884725	...	155.81	12.8733	0.03295	10.53	262	<1.06	2.25	6.5	< 9.70
587735349086912675	181028	126.597	8.42377	0.04594	11.17	205±11	0.62±0.09	2.67	3.6	9.77±0.06
587736478124408901	...	209.255	11.6114	0.03870	10.72	332	<1.19	2.25	6.5	< 9.89
587736802935373840	...	196.764	13.637	0.02727	10.23	312	<1.16	2.25	6.5	< 9.57
587736813672202319	...	237.478	9.82864	0.04587	10.92	404	<1.32	2.25	6.5	<10.08
587738409251635215	190666	150.264	11.4614	0.03629	10.34	225±8	3.17±0.09	2.30	20.5	10.28±0.01
587738410860806225	190505	146.827	12.1585	0.04751	10.75	216±6	1.07±0.08	2.25	7.3	10.04±0.03
587738411401412648	...	155.398	13.7755	0.04554	10.91	389	<1.29	2.25	6.5	<10.06
588010359073931336	201281	151.836	4.07931	0.02859	10.48	358±10	1.28±0.11	2.48	6.1	9.69±0.03
588010360148656136	200217	154	4.95476	0.03203	10.02	325±6	1.72±0.10	2.33	9.2	9.91±0.02
588010879841992790	231357	201.04	5.25972	0.02489	9.81	229±4	2.33±0.09	2.31	14.9	9.83±0.02
588010880371654746	220306	184.483	5.86978	0.02347	9.72	287±31	2.01±0.11	2.57	10.3	9.71±0.02
588017569779744827	...	203.101	11.1064	0.03146	10.06	302	<1.14	2.25	6.5	< 9.69
588017702921633970	...	159.469	10.7583	0.05251	10.99	432	<1.42	2.25	6.5	<10.23
588017702940049506	232401	202.338	11.3365	0.04771	10.40	329±14	1.20±0.12	2.60	5.7	10.09±0.04
588017703471611920	...	189.9	12.4389	0.04086	10.76	383	<1.28	2.25	6.5	< 9.97

The AGC number refers to the ALFALFA catalog number and exists only for detections. W_{50} is the FWHM of the 21 cm emission line for detections and derived from the *i*-band Tully-Fisher for non-detections. S_{21} is the integrated 21 cm line flux. Derivations of the RMS and S/N are given in Haynes et al. (2011) and are set to 2.25 mJy and 6.5 for non-detections (ALFALFA.40 limits). Stellar masses are taken from the single Sersic fits of Mendel et al. (2014).

al. (2011) and are set to 2.25 mJy and 6.5 for non-detections in the ALFALFA.40 sample.

2.3 Control Sample

In order to investigate differences between the post-mergers and the general population, it is necessary to define a control sample of undisturbed galaxies (defined as having a Galaxy Zoo merger vote fraction of zero) with no close com-

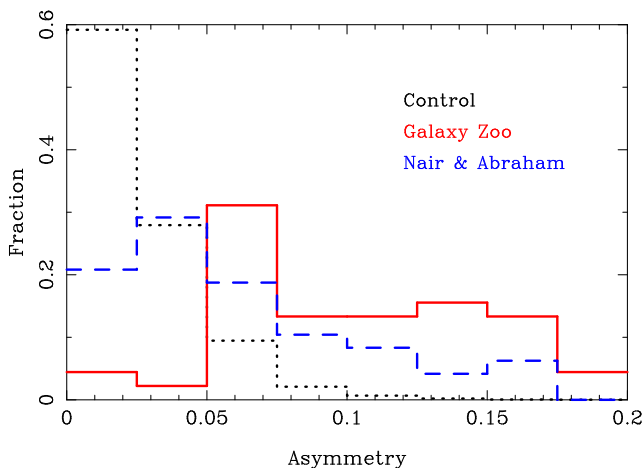


Figure 2. The distribution of asymmetry (R_A) parameters in the 45 Galaxy Zoo post-mergers and 48 post-mergers from Nair & Abraham (2010) with HI mass measurements, plus the combined control sample (red, blue dashed and black dotted histograms respectively). Whereas the Galaxy Zoo post-merger sample has very few mildly asymmetric galaxies ($R_A < 0.05$), the Nair & Abraham sample includes galaxies with much more subtle asymmetries. Both post-merger samples have significantly higher asymmetries than the control sample.

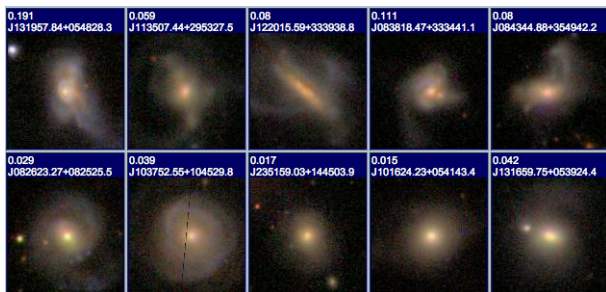


Figure 3. Examples of highly asymmetric ($R_A > 0.05$) galaxies in the Galaxy Zoo sample (top row) and smoother ($R_A < 0.05$) galaxies from the Nair & Abraham supplementary sample in the lower row. The value of R_A is given at the top of each panel.

panion (e.g. Ellison et al. 2013a,b). The control sample is compiled by matching non-merger galaxies simultaneously in stellar mass, redshift and environment². Following our previous works, we compute local environmental densities, Σ_n :

$$\Sigma_n = \frac{n}{\pi d_n^2}, \quad (3)$$

where d_n is the projected distance in Mpc to the n^{th} nearest neighbour within $\pm 1000 \text{ km s}^{-1}$. Normalized den-

sities, δ_n , are computed relative to the median Σ_n within a redshift slice ± 0.01 . In this study we adopt $n = 5$. The tolerance for matching is 0.005 in redshift, 0.1 dex in stellar mass and 0.1 dex in normalized local density. If less than five matches are found, the tolerance is grown by a further $\Delta z = 0.005$ in redshift, $\Delta \log M_* = 0.1$ dex in stellar mass and $\Delta \delta_5 = 0.1$ dex in normalized local density until the required number of matches is achieved.

The control matching accounts for various intrinsic dependences and observational biases. Perhaps most importantly, it has been shown that HI mass correlates well (although with significant scatter) with stellar mass (Fabello et al. 2011; Cortese et al. 2011; Catinella et al. 2012). Looking for deviations in the typical HI content therefore needs to take this scaling into account. Due to the fixed exposure time of the ALFALFA survey, the HI detection threshold is strongly distance dependent (Haynes et al. 2011), necessitating the redshift matching. Finally, the environmental matching mitigates biases due to contamination by other galaxies in the Arecibo beam (although manual rejection of cases with obvious beam contamination are performed as part of the catalog assembly), as well as any dependence of gas fraction on group or cluster membership, or other environmental trends (e.g. Solanes et al. 2001; Kilborn et al. 2009; Chung et al. 2009; Cortese et al. 2011; Fabello et al. 2012; Catinella et al. 2013; Hess & Wilcots 2013).

2.4 Sample comparison

The final post-merger sample used in this paper is the combination of the Ellison et al. (2013a) Galaxy Zoo sample and the Nair & Abraham (2010) supplementary sample, and contains 93 post-mergers with HI masses (43 galaxies) or limits (50 galaxies). A summary of the number of targets in each sub-sample is given in Table 4. In Figure 2 we compare the asymmetries of the Galaxy Zoo and supplementary Nair & Abraham (2010) samples that have ALFALFA.40 matches. The asymmetries are determined from the GIM2D bulge+disk decompositions of SDSS galaxies performed by Simard et al. (2011). In particular, we use the R_A parameter (measured in the r -band), which measures the fraction of light in the residual image (after subtraction of the bulge and disk) that remains after a 180 degree subtraction of itself (see equation 11b in Simard et al. 2002). R_A is therefore the residual asymmetric component.

Figure 2 reveals that the Galaxy Zoo post-merger sample is dominated by galaxies with strong asymmetries ($R_A > 0.05$). Although some highly asymmetric galaxies do exist in the supplementary sample³, it is clear that it contains a significant population of galaxies with $R_A < 0.05$. For comparison, the asymmetries of the control galaxies are also shown in Fig. 2; 60 per cent of the control galaxies have $R_A < 0.02$, a regime little populated by the post-mergers. Figure 3 shows some examples of galaxies with different asymmetries. In the top row we show five of the Galaxy Zoo sample with $R_A > 0.05$ and in the bottom row five of

² Unfortunately, without precise information on the progenitor morphologies, it is not possible to account for Hubble type in the matching process.

³ Recall that the Nair & Abraham (2010) supplementary sample of post-mergers is checked against the Galaxy Zoo sample and duplicates excluded. The supplementary sample therefore has had some of its more asymmetric galaxies excluded.

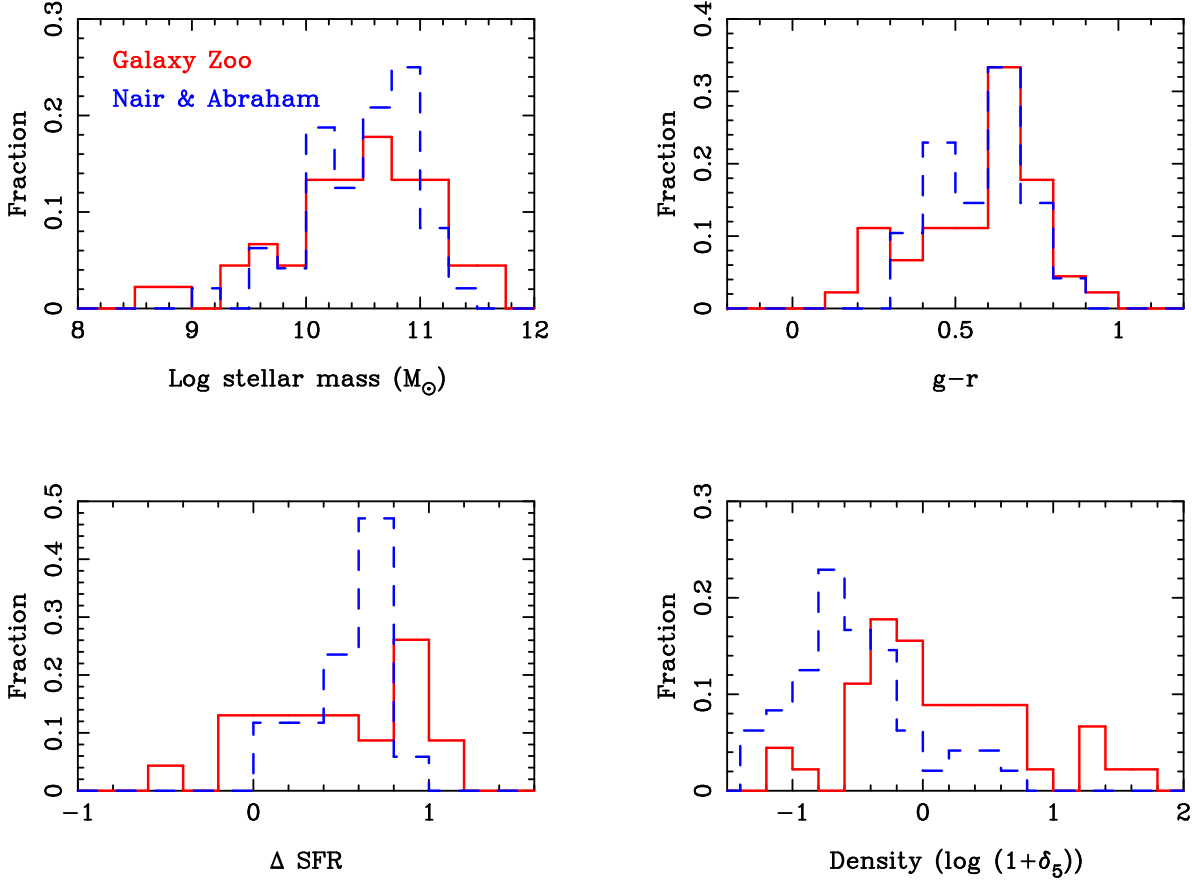


Figure 4. A comparison between the properties of the Galaxy Zoo post-merger sample and the Nair & Abraham supplementary sample (red and blue-dashed histograms respectively) for which we have HI measurements. Top left panel: Total stellar masses are taken from Mendel et al. (2014). Top right panel: Extinction and k-corrected Petrosian $g-r$ colours. Bottom left panel: SFR enhancements. Bottom right panel: normalized local densities.

Table 4. The number of post-mergers in each sub-sample

Selected from:	Ellison et al. (2013a) / Galaxy Zoo	Nair & Abraham (2010)
Total	45	48
HI detections	20	23
Above ALFALFA.40	15	16
90% completeness		

the Nair & Abraham galaxies with $R_A < 0.05$. The value of R_A is given at the top of each panel.

From simulations of galaxy mergers, it has been shown that the visual properties of post-mergers depend on timescale, the initial galactic properties, merger geometry and mass ratio (Lotz et al. 2008, 2010a,b; Ji et al 2014). For example, Lotz et al. (2010a) have demonstrated that higher gas fraction galaxies exhibit longer-lived tidal fea-

tures and disturbed morphologies. Conversely, ‘dry mergers’, those with low gas fractions, will exhibit lower surface brightness, less dramatic, and shorter-lived features. Post-mergers with lower asymmetries (i.e. smoother morphologies) may therefore be the result of lower gas fraction mergers, or they may simply be older. Trends of gas fraction with galaxy asymmetry are discussed later in this paper.

The properties of the two post-merger samples are further explored in Fig. 4. Recall that some of the post-mergers in the Nair & Abraham (2010) catalog are also identified by Galaxy Zoo and duplicates are removed from the supplementary sample. The supplementary sample of post-mergers presented here represents only those galaxies uniquely identified by Nair & Abraham (2010). The top left and right panels of Fig. 4 show that the stellar mass and Petrosian $g-r$ colour distributions are similar between the two samples. The bottom left panel of Fig. 4 compares, for galaxies classified as star-forming, the SFR enhancements, relative to th mass-, redshift and environment-matched control sample

described in Section 2.3 (Δ SFR, see Ellison et al. 2013a,b for more details). In brief, Δ SFR compares the SFR of the post-merger with that of its control sample:

$$\Delta SFR = \log SFR_{PM} - \log SFR_{control}, \quad (4)$$

such that, for example, a factor of two enhancement in SFR yields a Δ SFR = 0.3. The median SFR enhancement is 0.41 for the Galaxy Zoo postmergers, but 0.62 for the Nair & Abraham sample. Moreover, there are no galaxies in the latter sample with a negative Δ SFR (lower SFRs than the matched control). However, the *fraction* of star-forming galaxies is significantly lower in the Nair & Abraham sample: 35 per cent, compared with 52 per cent amongst the Galaxy Zoo postmergers.

There is also a difference in the local environments of the two samples, as shown in the lower right panel of Fig. 4, with postmergers in the supplementary sample systematically located in regions of lower galactic density. However, as noted above, the procedure for sample selection and removing duplicates means that a comparison of galaxy properties between the two samples is not strictly based on physical properties (an analysis that we perform later in this paper). Nonetheless, the above statistics and Figs 2 – 4 demonstrate that the two visually selected samples identify galaxies with different properties, despite being selected from the same imaging data.

2.5 Completeness

Of the 93 postmergers presented in this study, 37 have new HI mass measurements from our Arecibo observations. It is interesting to compare the sensitivity of these new observations to that of the ALFALFA survey. As described in Haynes et al. (2011), the completeness of the ALFALFA survey is basically a function of the expected FWHM of the 21cm line, W_{50} . From equation 4 of Haynes et al. (2011), we have that the 90% completeness of code 1 sources ($S/N > 6.5$) is given as

$$\log S_{21} = \begin{cases} 0.5 \log W_{50} - 1.14, & \text{if } \log W_{50} < 2.5 \\ \log W_{50} - 2.39, & \text{if } \log W_{50} \geq 2.5 \end{cases} \quad (5)$$

In Fig 5, we show the measured fluxes of ALFALFA.40 code 1 sources, with the 90% completeness limit shown. We show in red the 45 measurements of Galaxy Zoo postmergers (8 of which are taken from ALFALFA.40), and in blue we show the 48 measurements from ALFALFA.40 of the postmergers from the Nair & Abraham (2010) catalog. It is clear that some of our new observations are deeper than the completeness limit of ALFALFA, which is to be expected from our observation strategy. In the following analysis, we will frequently consider only those postmergers that lie above the completeness limit, in order to make fair statistical comparisons between the gas content of the postmergers and isolated (non-merger) galaxies. However, for the rest of this analysis, we will combine the supplementary Nair & Abraham sample with the Galaxy Zoo post-merger sample. We hereafter refer to this simply as ‘the post-merger’ sample; it contains 93 galaxies, of which 43 have HI detections and 31 are above the ALFALFA.40 90% completeness

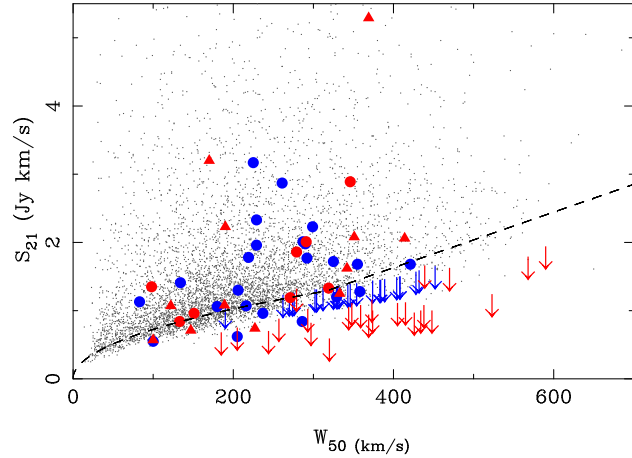


Figure 5. The 21 cm flux (S_{21}) as a function of the FWHM (W_{50}). The black dashed line shows the 90% completeness of the ALFALFA.40 catalog, as given by Haynes et al. (2011), see Eqn 5. ALFALFA.40 (non-merger) galaxies are shown in grey. Postmergers are shown in red and blue for the Galaxy Zoo (Ellison et al. 2013a) and Nair & Abraham (2010) samples, respectively. Of the 45 Galaxy Zoo postmergers, new detections are shown with red triangles, new limits are shown with red arrows and matches to ALFALFA.40 are shown with red circles. All of the Nair & Abraham (2010) postmergers have detections taken from ALFALFA.40, and are therefore all shown with circles.

limit (Table 4). Although we have shown that the properties of these samples differ, their properties overlap and the distinction between them has no clean physical boundary. Later in this work, we will investigate how gas fractions depend on galaxy properties within this combined sample.

3 RESULTS

3.1 Gas fractions

The HI gas fraction (hereafter simply ‘gas fraction’) is defined in this work as $f_{gas} = M_{HI} / M_{\star}^4$. In Figure 6 we present the HI masses and gas fractions for the full post-merger sample. For comparison, we also show non-merger galaxies detected in the ALFALFA.40 sample. The isolated (non-merger) nature of these galaxies is determined by requiring that the Galaxy Zoo merger vote fraction be zero, and we further require that the ALFALFA ocode=1 and Ngal=1, indicating that only one SDSS source has been matched. For clarity, only ALFALFA detections (not upper limits) are shown. Figure 6 shows that the galaxies in our post-merger sample are biased towards the high mass end of the galaxy distribution for which ALFALFA HI masses exist. Figure 6 also shows that some of our own Arecibo

⁴ In theoretical works, it is more common to define $f_{gas} = M_{HI} / M_{total}$, but we adopt the more frequently used definition in observational studies.

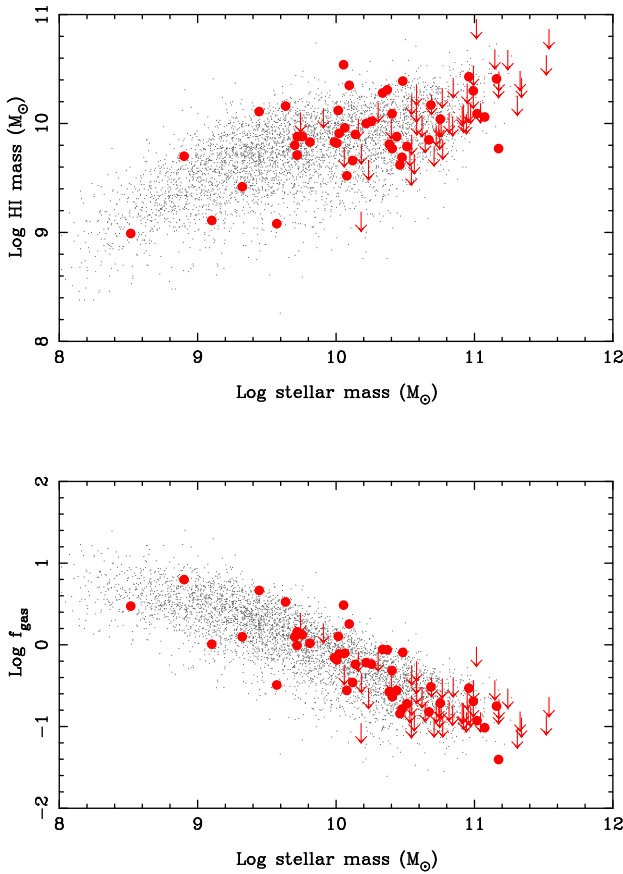


Figure 6. The HI mass (top panel) and HI gas fraction (bottom panel) as a function of stellar mass. Red points (and upper limits) represent measurements for the post-merger sample and small grey points are non-merger galaxies extracted from the ALFALFA.40 data release (see text for details).

observations are deeper than the typical ALFALFA.40 detections (see also Figure 5), whose effective integration times are only 40 seconds (recall that ALFALFA upper limits are not shown to avoid crowding).

In order to make a more fair comparison between the post-mergers and ALFALFA.40, Fig. 7 shows the same data as in Fig. 6 but with only those galaxies that pass the 90% completeness threshold included. In order to test statistically whether post-mergers exhibit distinct gas fractions from isolated galaxies, we will define a galactic ‘gas fraction offset’, Δf_{gas} , which quantifies a gas fraction relative to isolated (control) galaxies with otherwise similar properties. The Δf_{gas} metric is very similar in spirit (although opposite in sign) to the widely used HI deficiency (e.g. Haynes, Giovanelli & Chincarini 1984). The application of such ‘offset’ techniques has been previously used to effectively quantify differences in colour, SFR (e.g. Fig. 4), metallicity and active galactic nuclei (AGN) frequency between galaxy pairs and non-mergers (e.g. Patton et al. 2011, 2013; Ellison et al. 2010, 2011b; Scudder et al. 2012; Satyapal et al. 2014).

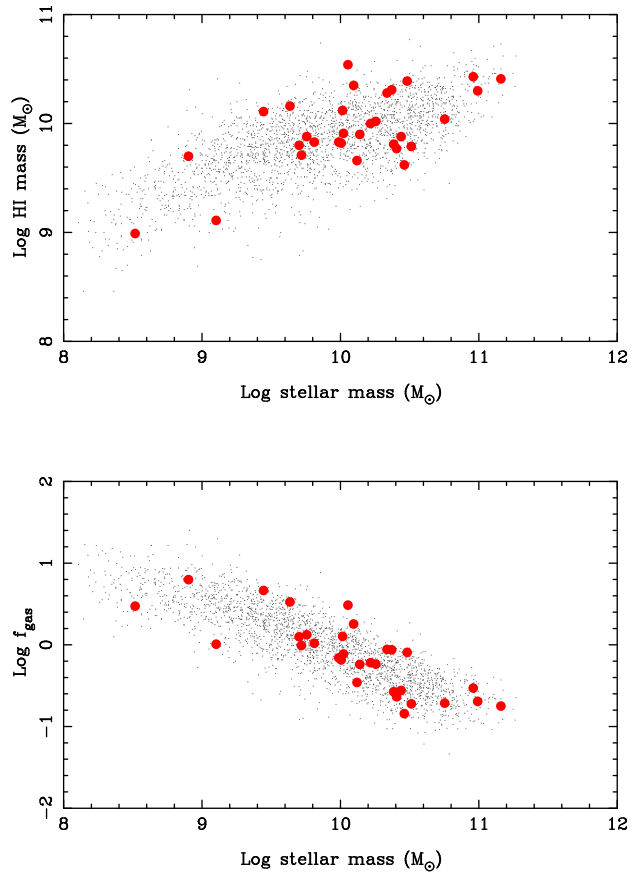


Figure 7. As for Fig. 6, but only showing galaxies with HI detections that are above the ALFALFA.40 90% completeness limit.

3.2 Gas fraction offsets

The basic procedure for control matching is described in Section 2.3, although we now additionally require that both the post-merger, and galaxies in the control ‘pool’ lie above the ALFALFA completeness threshold, as defined in equation 5. There are 31 post-mergers that fulfill this criterion (see Table 4) and can hence have robust gas fraction offsets quantified. Mergers that lie below the completeness threshold will appear to have spuriously low HI masses for their stellar mass, due to the lack of ALFALFA galaxies in this regime. As described in Section 2.3, the control sample is assembled by simultaneously matching in stellar mass, redshift and local environment all ALFALFA galaxies that are also above the 90% completeness threshold. By definition, this is the majority, but not all, of the published ALFALFA.40 sample. As described in Section 2.3, we require a minimum of 5 control galaxies for each post-merger; if this minimum is not reached, the matching tolerances are grown. In practice, there are typically 10 – 30 controls for each post-merger.

From the matched control sample it is then possible to calculate a gas fraction offset defined as

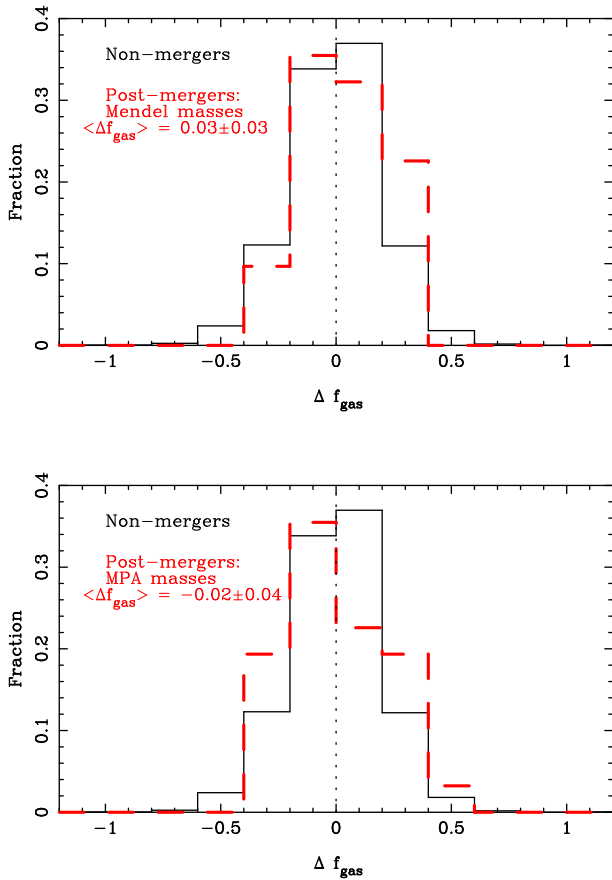


Figure 8. Distribution of gas fraction offsets. In both panels, the solid black histogram shows the distribution of Δf_{gas} for isolated ALFALFA galaxies and the red dashed histograms indicate the post-merger sample. In the top panel, the stellar masses of post-merger galaxies are taken from the Mendel et al. (2014) catalog. In the lower panel, stellar masses are taken from the MPA catalog (Kauffmann et al. 2003).

$$\Delta f_{\text{gas}} = \log f_{\text{gas,PM}} - \log f_{\text{gas,control}}, \quad (6)$$

where the control value is the median of the matched control galaxy gas fractions for a given post-merger. This calculation is only made for galaxies with detections above the ALFALFA.40 90 per cent completeness threshold. A value of $\Delta f_{\text{gas}} = 0$ therefore indicates that a galaxy has an HI gas content that is typical for its mass, redshift and local density. In contrast, positive and negative values of Δf_{gas} indicate gas-rich and gas-poor galaxies respectively. We can also calculate gas fraction offsets for isolated ALFALFA galaxies, by again comparing their gas fractions with other isolated galaxies at the same mass, redshift and local density.

The top panel of Figure 8 shows the distribution of Δf_{gas} amongst isolated ALFALFA galaxies (black histogram) and the post-merger sample (red dashed histogram). For the post-merger galaxies that are above the

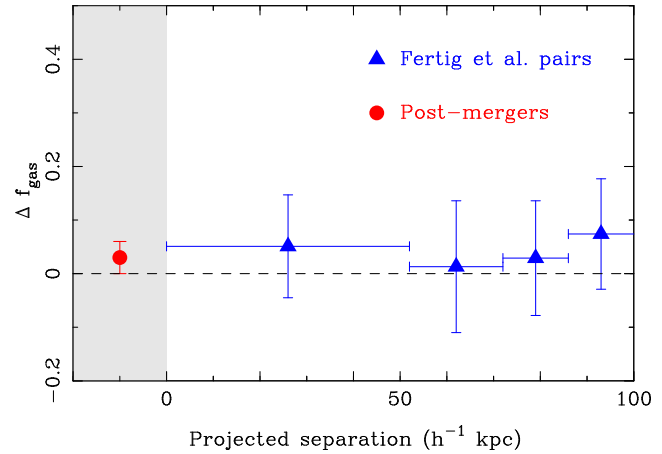


Figure 9. Distribution of mean gas fraction offsets as a function of projected separation for the pairs sample of Fertig et al. (2015, blue triangles) and the post-mergers (red circle located in the grey shaded box) presented in this paper. There is no indication for significant gas consumption at any stage during the merger.

ALFALFA.40 completeness threshold the distribution of gas fraction offsets is very similar to the values observed in isolated galaxies. The mean gas fraction offset in the post-mergers is consistent with no merger-induced change in the atomic gas fraction: $\Delta f_{\text{gas}} = 0.03 \pm 0.03$.

Since the gas fraction combines both HI masses and stellar masses by definition, it is germane to consider whether the gas fraction results depend sensitively on the derivation of M_* . We have adopted the single Sérsic fits from Mendel et al. (2014), which include the numerous improvements to SDSS photometry detailed in Simard et al. (2011). However, there are two possible concerns with these masses that are relevant to the study of post-mergers. First, a single Sérsic fit does not account for flux in the asymmetric components of the light, which might be a significant fraction in post-mergers. Second, the Mendel masses do not include star formation histories with bursts. Although smooth star formation histories are a good average representation of the general galaxy population, this is not likely to be the case for mergers, which are known to exhibit bursts of star formation following close passages and at coalescence. For comparison, we therefore repeat the Δf_{gas} analysis with masses derived by Kauffmann et al. (2003) (hereafter ‘MPA masses’) that are based on total photometry and include bursty star formation histories. The comparison between values of Δf_{gas} for the ALFALFA.40 sample and post-mergers derived from matching MPA masses, rather than Mendel masses, is shown in the lower panel of Fig. 8. Although the individual values of Δf_{gas} in the post-mergers are slightly different, the distribution of values in the post-merger sample remains very similar to the isolated sample. The mean gas fraction offset is also still consistent with the matched control sample: $\Delta f_{\text{gas}} = -0.02 \pm 0.04$.

Fertig et al. (2015) have recently used similar methods to ours to study the gas fraction offsets in galaxy pairs.

The only notable difference in their analysis (apart from the selection of pairs, rather than post-mergers) is that their control sample is composed of wide pairs, rather than truly isolated galaxies. The use of wide pairs as controls has been previously used in the literature (e.g. Scott & Kaviraj 2014) and Fertig et al. (2015) show that this is a robust approach for gas fractions. Therefore, although Fertig et al. (2015) use wide pairs, and this work uses isolated non-mergers, for the control sample, the methodology is otherwise identical and the results should be comparable.

Fertig et al. (2015) found no difference between the gas fractions in the close and wide pairs, indicating that consumption is not significant in the pre-merger phase of the interaction. In Fig. 9 we combine the results of Fertig et al. (2015) with our post-mergers, in order to provide a complete view of HI gas consumption during the merger process. The blue points show the gas fraction offsets as a function of projected separation in the Fertig et al. (2015) pairs sample. The filled red point is the mean Δf_{gas} in the combined post-merger sample (Fig. 8). None of the observed data points are located at $\Delta f_{gas} < 0$, indicating a lack of measured gas consumption throughout the merger stages probed by our samples.

3.3 Detection fractions

In order to make a fair comparison between the post-merger sample and our control sample (drawn from ALFALFA.40), it was necessary to impose a consistent detection threshold for both samples. Although this leads to a robust and fair comparison, the analysis of Δf_{gas} includes only one third of our sample galaxies. Therefore, whilst we can state that, for galaxies detected in HI above the ALFALFA threshold the typical HI gas fraction is consistent with isolated galaxies, we have not yet investigated the nature of the rest of the sample. It is possible, for example, that whilst some galaxies possess ‘normal’ gas fractions, the majority of post-mergers are actually depleted, and that this depletion is the main reason they are below our detection limit.

In the absence of a deeper control sample, it is not possible to quantify the depletion in either the detections that are below the ALFALFA.40 threshold (of which there are 12), nor in the non-detections. However, we can compute the detection fractions of the post-mergers and compare it to that of the control, in order to judge whether the former are more frequently gas-poor. For this calculation, we re-make the control sample, identifying the single best match (minimized deviation in stellar mass, redshift and local density) for each post-merger. This adjustment is necessary due to the different number of control galaxies per post-merger permitted by the original procedure. The detection fraction is defined as the fraction of galaxies above the ALFALFA detection threshold (equation 5), such that this calculation is not affected by the higher sensitivity of some of our Arecibo observations. We find that the detection fraction of post-mergers is almost double that of the control (32 ± 6 per cent versus 17 ± 4 per cent). The result is not sensitive to the number of controls required in the matching process (i.e. similar results are obtained with 5 matches).

The high detection fractions measured amongst the full post-merger sample again support the lack of a dominant population of gas depleted galaxies. On the contrary, the

factor of two enhancement in the post-merger HI detection fraction may indicate that either the post-merger galaxies have a higher tendency to contain *some* gas, or that their gas fractions have been preferentially boosted above the nominal ALFALFA completeness threshold. These possibilities can be reconciled with the gas fraction result (which yielded an average post-merger Δf_{gas} consistent with zero) by recalling that ALFALFA is a shallow survey that itself consists of relatively gas-rich members of the galaxy population. Our measurement of gas fraction offsets may therefore be an under-estimate of the true values⁵. Therefore, not only is there no evidence for gas consumption in the post-mergers based on direct comparison of the observed gas fractions in the control and post-merger sample (Fig 8, but our analysis of the HI mass detection fractions hint that post-mergers may actually be somewhat gas-rich. This possibility is explored further below in Section 4.

3.4 Dependence of Gas Fraction Offset on Asymmetry

It is well known that post-mergers are most asymmetric soon after coalescence, and that tidal features will fade with time thereafter (e.g. Lotz et al. 2008), so that mergers selected from shallow imaging surveys will be biased towards recently coalesced galaxies (Ji et al. 2014). In addition to the effects of merger timing, the nature of the progenitor galaxies can affect the resulting asymmetries. For example, the simulations of Lotz et al. (2010a) show that smoother merger remnants result from more gas-poor mergers.

In Fig. 2 we showed that there is a range of asymmetries in our post-merger sample, with a bias towards the highest values in the Galaxy Zoo sample from Ellison et al. (2013a). Indeed, in Ellison et al. (2013a) we argued that these galaxies were only recently coalesced based on their low gas phase metallicities. It is therefore interesting to investigate whether there is a trend of gas consumption with asymmetry, as might be expected if the least disturbed post-mergers are older.

In the top panel of Fig. 10 we plot Δf_{gas} as a function of *r*-band asymmetry for the ALFALFA.40 complete post-merger sample. There is no obvious trend between asymmetry and gas fraction offset. In the lower panel we plot the distribution of Δf_{gas} for high ($R_A \geq 0.07$, red histogram) and low ($R_A < 0.07$, blue histogram) asymmetry post-mergers, relative to the median asymmetry of the sample. Based on the results of a Kolmogorov-Smirnov (KS) test, there is no statistical difference that the two asymmetry samples have different distributions of Δf_{gas} .

An important caveat to the application of asymmetry metrics to mergers is their relative insensitivity to extended low surface brightness features. Adapting classic asymmetry indices to be more sensitive to such low surface brightness

⁵ The same caveat is applied to measurements of other properties of mergers investigated with matched control samples, due to the intrinsic nature of detection thresholds. For example, Scudder et al. (2012) caution that the SFR enhancements in their sample of galaxy pairs may be under estimates if their control sample contains (isolated) galaxies which themselves have preferentially elevated SFRs that boost them across the detection threshold.

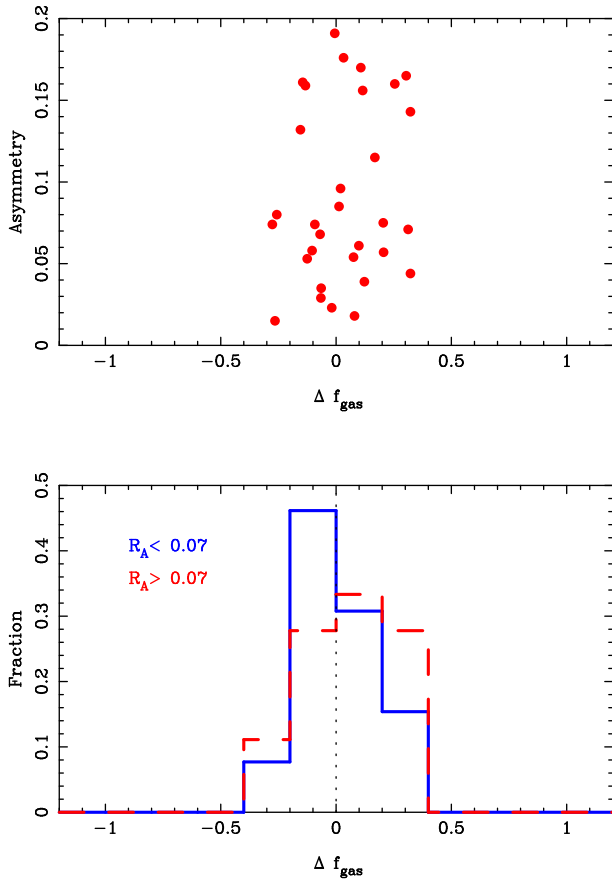


Figure 10. Top panel: Gas fraction offsets as a function of galaxy asymmetry for the post-merger sample. Bottom panel: Distribution of Δf_{gas} for post-mergers split by asymmetry at $R_A = 0.07$; the red and blue histograms show high and low asymmetry galaxies respectively.

features, particularly at large galactocentric radii, may help reveal a closer connection with changes manifest in galactic stellar and gaseous properties (e.g. Lelli et al. 2014; Pawlik et al., in prep.).

4 DISCUSSION

One of the main goals of the work presented here is to tackle the question of whether the merger process significantly depletes the gas reservoir of the remnant. We have found no evidence of this in the measured HI gas fractions of our sample of post-merger galaxies. Specifically, based on HI detections in 31 galaxies for which we can identify a fair control sample from ALFALFA, we find that post-mergers have gas fractions that are indistinguishable from equivalent isolated galaxies. However, due to the shallow nature of the ALFALFA.40 survey, the sample from which the controls are drawn is dominated by relatively gas-rich galaxies. Indeed, considering the full sample of 93 post-mergers, we find an HI detection fraction that is double that of the control sample of isolated galaxies. Therefore, contrary to finding evidence for

gas consumption, our analysis of HI gas fraction enhancements suggests that post-mergers might be relatively gas-rich. A number of other observational studies have drawn similar conclusions (Braine & Combes 1993; Bettoni et al. 2001; Huchtmeier et al. 2008; Stark et al. 2013; Goncalves et al. 2014). Previous simulations have proposed that mergers might renew their cold gas reservoirs through the cooling of hot halo gas (Moster et al. 2011; Tonnesen & Cen 2012). Indeed, recent cosmological simulations measured increases in the HI gas fraction of ~ 20 per cent within a few hundred Myr after a merger (Rafiee-anto et al. 2014).

However, despite the theoretical predictions for enhanced gas fractions, there may be a more mundane way to create high gas fractions in recent post-mergers, originating from the declining gas fractions with increasing stellar mass, as shown in Figure 6 (and see also Catinella et al. 2012 and references therein). The simple addition of two randomly chosen galaxies in such a distribution will yield relatively high gas masses for a given stellar mass. We demonstrate this effect in Figure 11 with a simple simulation. We draw 2000 galaxies at random from ALFALFA.40, pairing them up by adding their stellar masses and gas masses to yield ‘measurements’ of f_{gas} for 1000 fake post-mergers. For each of these fake post-mergers, we assemble a control sample matched in stellar mass and determine Δf_{gas} as described above⁶. For reference, Figure 11 again shows (black histogram) the distribution of Δf_{gas} for all ALFALFA.40 galaxies above the 90% completeness limit that also appears in the two panels of Figure 8. The red dashed histogram shows the distribution of the 1000 fake post-mergers, that are seen to be offset towards positive values with a mean $\Delta f_{gas} = 0.17 \pm 0.01$. This is a direct consequence of the combination of matching a control sample in stellar mass and the declining gas fractions with that same quantity.

Interestingly, the histograms shown in Fig. 11 are qualitatively similar to the results of Rafiee-anto et al. (2014), who compare the gas fractions of recently merged galaxies to non-mergers in a cosmological simulation and find a 20 per cent increase in the former. We stress that the gas fraction enhancement seen due to this ‘summation’ effect depends on the gas fractions of the progenitor galaxies, and also on the distribution of gas fractions in their controls. If pre-merger galaxies have initially higher gas fractions, the resulting Δf_{gas} of the post-merger will also be shifted to more positive values. Our simulation of fake post-mergers is therefore illustrative of the qualitative offset towards enhanced gas fractions that might be expected due to stellar mass matching.

The elevated HI detection fraction (by a factor of two) in our post-mergers compared with isolated controls of the same stellar mass may plausibly be explained by this effect. However, we see no net shift towards positive Δf_{gas} (Fig 8) as indicated might be expected by Fig. 11. As proposed above, the consistency between post-merger and control gas fraction offsets may be due to a tendency for the controls themselves to be relatively gas-rich, which artificially reduces the magnitude of the measured gas fraction enhancement. An alternative explanation for the lack of gas

⁶ For the real post-mergers, we also match in redshift and environment, but this is not possible in this simulation.

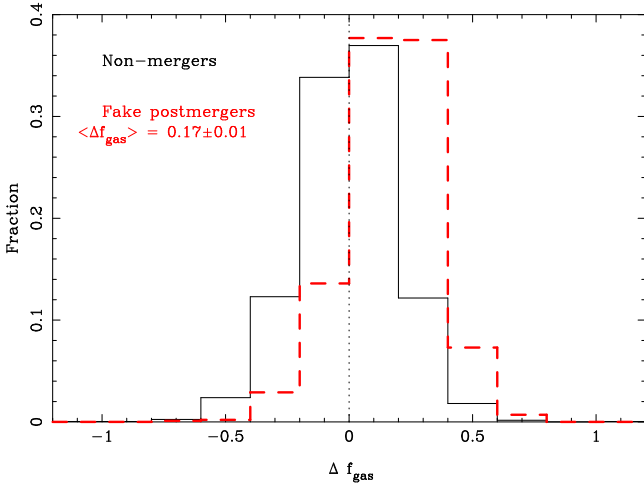


Figure 11. Distribution of gas fraction offsets for isolated ALFALFA galaxies (solid black histogram) and 1000 fake postmergers (red dashed histogram), constructed through random draws from the ALFALFA.40 sample. Due to the declining gas fraction as a function of stellar mass, matching in stellar mass leads to a shift towards positive values of Δf_{gas} .

fraction enhancement in the observations is that prompt consumption of the initial HI excess has already occurred in the post-mergers due to high rates of star formation. In order to quantify the expected amount of gas consumption in the post-mergers phase, we turn now to a suite of binary merger simulations.

4.1 Timescales for Gas Depletion

Fig. 11 demonstrates that, in a stellar mass matched sample, the trend of declining f_{gas} with M_* leads to a shift towards high gas fraction offsets when two galaxies are combined. Moreover, accretion of new cold gas is predicted by some merger simulations (e.g. Moster et al. 2011; Tonnesen & Cen 2012), and also might be expected in generic scenarios of mixing a cool and ionized medium (Marinacci et al. 2010; Marasco, Fraternali & Binney 2012). However, Fig. 8 shows that there is, on average, no enhancement in the gas fractions in the observed post-mergers. In this section, we explore whether the contrast between Figs. 8 and 11 is actually an indication of gas consumption.

A detailed assessment of gas consumption and recycling requires sophisticated hydrodynamical simulations that can adequately track the gas in its different phases (e.g. Davé et al. 2013), which is beyond the scope of this paper (but see Rafieferantsoa et al. 2014). However, we can make a rough assessment for a simplified case, based on the suite of merger simulations presented in Patton et al. (2013) using the model for radiative gas cooling, star formation, and feedback as summarized in Torrey et al. (2012). Such simulations will also provide an approximate timescale over which galaxies will return to their nominal scaling relations.

The suite of binary mergers includes 75 orbital variations of a merger with mass ratio $M_{*,1}/M_{*,2} = 1.4 \times 10^{10}$

$M_{\odot} / 5.7 \times 10^9 M_{\odot} = 2.5$, which represents the typical pairing in the SDSS sample of Patton et al. (2013). Two isolated galaxies, identical to each of the galaxies in the merger, which act as controls, are also simulated. By comparing the integrated SFR in mergers during the course of the simulation (which runs for a total of 6.5 Gyr), with the isolated controls, we can determine the typical additional stellar mass created in the merger (compared to the baseline stellar mass created in the controls), δM . Although this simulation does not track the various phases of gas, we make the simplifying assumption that star formation is initially fed from gas that originated as HI. This assumption leads to a conservative upper limit on the gas consumption.

In Fig. 12 we plot the accumulation of stellar mass throughout the 6.5 Gyr simulation for 3 out of 75 of our orbital variations, which include combinations of five eccentricities and five impact parameters for 3 relative disk inclinations (Patton et al. 2013; Moreno et al. 2015). The red, green and blue lines show examples from the e , f and k suites, which have relative disk orientations of 60, 90 and 180 degrees respectively (Robertson et al. 2006). The coloured dashed lines in the top panel shows the accumulated stellar mass in both galaxies in the merger, and the black line shows the mass build-up for identical galaxies evolved in isolation. The first (left-most) set of vertical dotted lines indicates the time of first peri-centre; this time is very similar for each of the 3 orbits. The second (right-most) set of vertical dotted lines shows the time of coalescence, which is more sensitive to the orbital parameters. The example e simulation (red line) is strongly affected by the first pericentric passage and significantly increases its stellar mass through triggered star formation after this time. However, it is little affected by coalescence. The opposite is true for the example k merger. Its anti-aligned disk means that it is little affected by the pericentric passage, but experiences a larger star burst at coalescence. The intermediate example, f , has modest star formation triggered at both peri-centre and coalescence (see Moreno et al. 2015 for a more detailed analysis of orbital and spatial dependences of triggered star formation). Despite these very different histories, the total accumulated stellar mass is very similar for these three examples. This general tendency for small pericentre starbursts to be followed by large bursts at coalescence, and vice-versa, was also observed in the large suite of merger simulations run by Di Matteo et al. (2007). In the lower panel of Fig. 12, we calculate the difference between the accumulated stellar mass in the mergers and that of the control galaxies. Again, the time at which the mass is formed is evidently dependent on the geometry, but converges to a similar value of $\sim 7 \times 10^8 M_{\odot}$ by the end of the simulation. Note that δM does not change much after 500 Myrs post-coalescence, indicating that even if there is a star burst at the time of the final merger, it is short-lived and gas consumption does not increase much further beyond the rate expected for the isolated galaxy. The range of δM (after 6.5 Gyr) amongst the full suite of 75 orbits spans 3×10^8 to $1 \times 10^9 M_{\odot}$, again, a relatively narrow range considering the different burst histories.

Having established a typical value of $\delta M = 7 \times 10^8 M_{\odot}$, we assign HI masses ($M_{\text{HI},1}, M_{\text{HI},2}$) to the galaxies by determining the best fit solution to the ALFALFA.40 data points shown in Fig. 7:

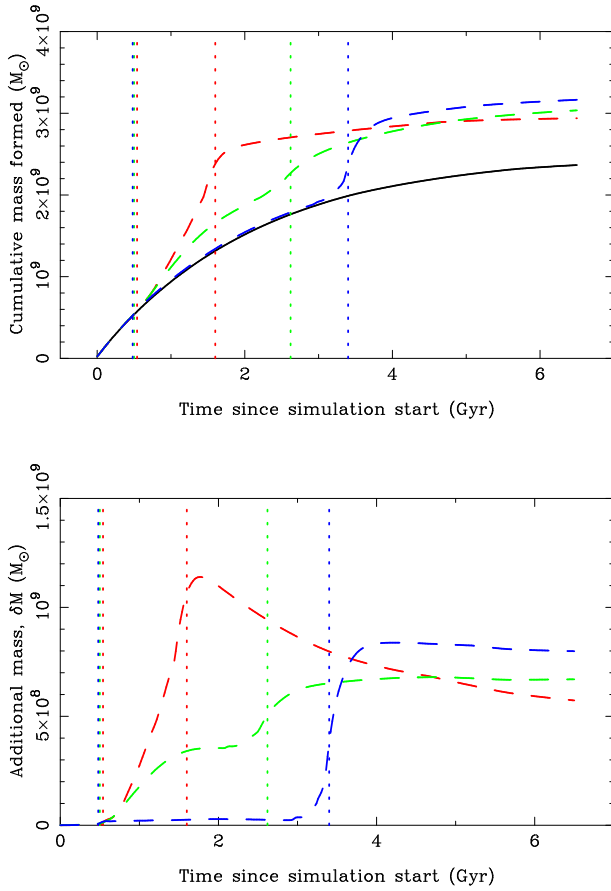


Figure 12. Top panel: Cumulative stellar mass formed in three example merger simulations from our suite of 75 orbital combinations of a 2.5:1 stellar mass ratio merger. The coloured dashed lines show the combined stellar masses made in both galaxies throughout the 6.5 Gyr simulation. Red, green and blue lines show examples from the e , f and k orientations respectively. The first (left-most) set of vertical dotted lines indicates the time of first pericentre. The second (right-most) set of vertical dotted lines shows the time of coalescence, which is sensitive to the orbital parameters. The black line shows the steady evolution of the isolated control galaxies. Bottom panel: The difference in stellar mass (δM) accumulated by the mergers relative to the control galaxies.

$$\log M_{HI} = 0.366 \log M_{\star} + 6.231. \quad (7)$$

The gas fraction of the post-merger is therefore given as

$$\log f_{gas,PM} = [\log(M_{HI,1} + M_{HI,2} - 2\delta M)] - [\log(M_{\star,1} + M_{\star,2} + 2\delta M)]. \quad (8)$$

The control galaxy gas fraction $f_{gas,c}$ is determined from

$$\log f_{gas,c} = \log(M_{HI,c}) - [\log(M_{\star,1} + M_{\star,2})]. \quad (9)$$

where $M_{HI,c}$ is again determined from the best fit ALFALFA.40 data for a stellar mass $\log(M_{\star,1} + M_{\star,2})$. In the

case of no star formation (i.e. akin to the simulation of random pairings shown in the lower panel of Fig 8) we find a mean $\Delta f_{gas} = 0.17$. Inserting the appropriate numbers into equations 8 and 9, we find $\Delta f_{gas} = 0.11$ where star formation is depleting gas over the course of the simulation. Therefore, for the typical pair represented by our merger suite, the expected decrease in Δf_{gas} even several Gyr after coalescence is very modest, only 0.06 dex. For comparison, Fertig et al. (2015) used the same set of simulations to estimate an expected decrease in Δf_{gas} of 0.04 dex in the close pairs phase of the merger.

Although based on simplified approximations, the results of our simulations lead to similar conclusions to the more sophisticated treatment of gas fractions in mergers by Rafieferantsoa et al. (2014), namely that galaxy mergers may yield a medium-to-long term shift towards high gas fractions in their remnants, before a modest decline. The results of these simulations indicate that the contrast between the expected shift to positive Δf_{gas} from the summation of galaxies (Fig. 11) and the lack of a shift in the observed post-mergers (Fig. 8) is not due to gas consumption. Instead, we favour a scenario in which the matching of control galaxies from the ALFALFA survey is biased towards gas-rich galaxies, which reduces the gas fraction enhancement. However, increased gas fractions (or gas presence) are nonetheless implied from the high HI detection fractions in the post-mergers.

5 CONCLUSIONS AND CLOSING REMARKS

HI mass measurements of 93 post-merger galaxies, visually selected from the Sloan Digital Sky Survey, are presented, including new Arecibo observations for 37 of the sample galaxies. The remaining HI masses are taken from the ALFALFA.40 sample (Haynes et al. 2011). Through a carefully controlled matching procedure with isolated (non-merger) galaxies selected from the ALFALFA.40 data release, and taking into account differences in completeness thresholds, we calculate the gas fraction offset, Δf_{gas} , which quantifies the relative gas richness of each post-merger. We also calculate the gas fraction offset for all (non-merger) ALFALFA.40 galaxies through the same matching procedure. Finally, we interpret our gas fraction results with the aid of a suite of 75 binary merger simulations.

Our conclusions are as follows:

- (i) The gas fractions in post-merger galaxies that are above the ALFALFA.40 completeness threshold are consistent with those measured in a mass-, redshift- and environment-matched control sample (Fig. 8). Combined with comparable measurements in galaxy pairs (Fertig et al. 2015), we find that the HI gas fractions in interacting galaxies are consistent with their controls throughout the merger sequence (Fig. 9), with no evidence for significant consumption of the neutral gas reservoir.
- (ii) There is no trend between the gas fraction enhancement and galaxy asymmetry (Fig. 10).
- (iii) The HI detection fraction in the full post-merger sample is approximately double the detection fraction of the isolated, matched control galaxies. Therefore, in addition to finding a lack of gas consumption, our results suggest that

post-mergers may be, on average, more gas rich than isolated galaxies.

(iv) Although high gas fractions in post-mergers have been predicted in several simulations (Moster et al. 2011; Tonnesen & Cen 2012; Bekki 2014; Rafiee-Rantsoa et al. 2014), we demonstrate that this enhancement is expected even in the absence of hot halo gas cooling, or the accretion of external gas. By drawing random pairs of galaxies from the isolated galaxies in the ALFALFA.40 sample we show that high gas fractions may arise naturally from the pairing of two galaxies drawn at random from the ALFALFA.40 detections, due to the declining f_{gas} with increasing stellar mass of the underlying population (Fig. 11). Indeed, the results of this test indicate that for a stellar mass matched sample we might expect to see a shift towards positive Δf_{gas} in post-mergers.

(v) Based on a suite of binary merger simulations, we compute a conservative upper limit for HI gas consumption for a galaxy interaction that is representative of the SDSS pairs sample (Fig 12). We find that, even several Gyrs after coalescence, the impact of star formation on gas consumption is small and that Δf_{gas} is expected to change very little, decreasing by only 0.06 dex (although the exact consumption is likely to depend on mass ratios, orbital geometries etc.). Gas consumption therefore does not appear to explain the lack of gas fraction enhancement in the observations. Instead, we propose that our gas fraction offsets may be lower limits, due to the relatively gas-rich nature of the ALFALFA control sample.

We conclude that there is no evidence for significant gas consumption in our post-merger observations; on the contrary, the post-mergers may actually be somewhat gas-rich.

One remaining uncertainty in our investigation of the evolution of gas content in mergers concerns the molecular gas content. Measurement of the molecular component is not only necessary for obtaining a complete census of the galactic gas, but it is also critical for understanding the mode in which star formation is progressing. Highly star-forming galaxies at both high redshift and locally (e.g. the ULIRGs) are offset on the Kennicutt-Schmidt relation (Daddi et al. 2010a; Genzel et al. 2010). Mergers have been predicted to also inhabit this offset sequence that exhibits ten times higher SFR at fixed gas (total) mass surface density (Renaud et al. 2014).

Although numerous studies have investigated the detailed distribution of molecular gas in individual mergers (e.g. Yun & Hibbard 2001; Davis et al. 2013; Fernandez et al. 2014), a statistical study that combines HI and H₂, with a well defined control sample is required in order to quantify general trends within mergers. One possible reason for the lack of HI depletion in our merger sample, despite elevated rates of star formation, could be that the stars form from the extant molecular gas reservoir. However, the previous studies that have attempted to compare mergers and isolated galaxies have found that the molecular fraction is actually enhanced in mergers (Braine & Combes 1993; Bettoni et al. 2001; Stark et al. 2013). Further hints on the impact of the molecular gas reservoir in mergers may be gleaned from observations of local UV luminous galaxies, or ‘Lyman break analogs’ (LBAs) selected to have properties similar to normal star-forming galaxies at high redshift (Heckman

et al. 2005). Interestingly, the LBAs have many properties typical of local mergers, including high SFRs, low metallicities and large IR luminosities (Hoopes et al. 2007; Overzier et al. 2011). In a recent study of 6 LBAs, whose morphologies and emission line kinematics again indicate interactions, Gonçalves et al. (2014) found high CO fractions relative to ‘normal’ low redshift galaxies (Saintonge et al. 2011). Whilst some enhancement in the CO fraction may be expected from the simple addition of reservoirs, as we found for the HI gas fractions, it is also expected that the strong gas flows in mergers, that ultimately drive star formation, will also increase the CO fraction (Braine & Combes 1993). Conversely, Sargent et al. (2014) conclude that starburst galaxies (which are not necessarily mergers) have CO fractions that are typically 2–3 times lower than normal galaxies.

The measurement of normal HI masses, but elevated molecular fractions in a small sample of mergers led Braine & Combes (1993) to propose that, contrary to depleting the gas supply, interactions might be responsible for the cooling of ionized halo gas, which leads to a central build-up of H₂. Such a mechanism seems plausible theoretically, through the interaction of gas reservoirs (Marinacci et al. 2010; Moster et al. 2011; Tonnesen & Cen 2012; Marasco et al. 2012). Obtaining CO measurements for the post-mergers in our sample, and studying simultaneously the changes in the atomic and molecular gas components will therefore be an important complement to the study presented here.

ACKNOWLEDGMENTS

SLE and DRP acknowledge the receipt of an NSERC Discovery grant and DF and JLR acknowledge NSF grant AST-000167932 and a George Mason University Presidential Fellowship for support of this work. SLE is grateful to Trevor Mendel for discussions concerning stellar mass, to the astronomers at CEA-Saclay for hospitality during the final stages of this work and also to Paola Di Matteo, Gary Mamon, Florent Renaud, Pierre-Alain Duc, Stephanie Juneau and Frederic Bournaud for interesting merger-related discussions during her visit. We have also benefitted from discussions with Romeel Dave, Mark Sargent and Sheila Kannappan.

REFERENCES

- Alonso, M. S., Lambas, D. G., Tissera, P. B., Coldwell, G., 2006, MNRAS, 367, 1029
- Barton, E. J., Geller, M. J., & Kenyon, S. J., 2000, ApJ, 530, 660
- Bekki, K., 2014, MNRAS, 444, 1615
- Bell, E. F., et al., 2004, ApJ, 608, 752
- Bell, E. F., Zheng, X. Z., Papovich, C., Borch, A., Wolf, C., Meisenheimer, K., 2007, ApJ, 663, 834
- Bettoni, D., Galletta, G., Garcia-Burillo, S., Rodriguez-Franco, A., 2001, A&A, 374, 421
- Blake, C., et al., 2004, MNRAS, 355, 713
- Borch, A., et al. 2006, A&A, 453, 869
- Bothwell, M. S., Maiolino, R., Kennicutt, R., Cresci, G., Mannucci, F., Marconi, A., Ciccone, C., 2013, MNRAS, 433, 1425
- Bournaud, F., et al., 2011, ApJ, 730, 4
- Braine, J., & Combes, F., 1993, A&A, 269, 7
- Brooks, A. M., Governato, F., Quinn, T., Brook, C. B., Wadsley, J., 2009, ApJ, 694, 396

- Buyle, P., De Rijcke, S., Dejonghe, H., 2008, *ApJ*, 684, L17
 Carpineti, A., Kaviraj, S., Darg, D., Lintott, C., Schawinski, K., Shabala, S., 2012, *MNRAS*, 420, 2139
 Casasola, V., Bettoni, D., Galletta, G., 2004, *A&A*, 422, 941
 Catinella, B., et al, 2013, *MNRAS*, 436, 34
 Catinella, B., et al, 2012, *A&A*, 544, 65
 Chung, A., van Gorkom, J. H., Kenney, J. D. P., Crawl, H., Vollmer, B., 2009, *AJ*, 138, 1741
 Cortese, L., Catinella, B., Boissier, S., Boselli, A., Heinis, S., 2011, *MNRAS*, 415, 1797
 Daddi, E., et al. 2010a, *ApJ*, 714, L118
 Daddi, E., et al., 2010b, *ApJ*, 713, 686
 Darg, D. W., et al., 2010, *MNRAS*, 401, 1552
 Davé, R., Katz, N., Oppenheimer, B. D., Kollmeier, J. A., Weinberg, D. H., 2013, *MNRAS*, 434, 2645
 Davis, T. A., Heiderman, A., Evans, N. J., Iono, D., 2013, *MNRAS*, 436, 570
 Di Matteo, P., Combes, F., Melchior, A.-L., Semelin, B., 2007, *A&A*, 468, 61
 Di Matteo, P., Bournaud, F., Martig, M., Combes, F., Melchior, A.-L., Semelin, B., 2008, *A&A*, 492, 31
 Di Teodoro, E. M., Fraternali, F., 2014, *A&A*, 567, 68
 Ellison, S. L., Patton, D. R., Simard, L., McConnachie, A. W., 2008a *AJ*, 135, 1877
 Ellison, S. L., Patton, D. R., Simard, L., McConnachie, A. W., 2008b, *ApJ*, 672, L107
 Ellison, S. L., Patton, D. R., Simard, L., McConnachie, A. W., Baldry, I. K., Mendel, J. T., 2010, *MNRAS*, 407, 1514
 Ellison, S. L., Mendel, J. T., Patton, D. R., Scudder, J. M., 2013a, *MNRAS*, 453, 3627
 Ellison, S. L., Mendel, J. T., Scudder, J. M., Patton, D. R., Palmer, M. J. D., 2013b, *MNRAS*, 430, 3128
 Ellison, S. L., Nair, P., Patton, D. R., Scudder, J. M., Mendel, J. T., Simard, L., 2011a, *MNRAS*, 416, 2182
 Ellison, S. L., Patton, D. R., Mendel, J. T., Scudder, J. M., 2011b, *MNRAS*, 418, 2043
 Fabello, S., Kauffmann, G., Catinella, B., Giovanelli, R., Haynes, M. P., Heckman, T. M., Schiminovich, D., 2011, *MNRAS*, 416, 1739
 Fabello, S., Kauffmann, G., Catinella, B., Li, C., Giovanelli, R., Haynes, M., 2012, *MNRAS*, 427, 2841
 Faber, S. M., et al., 2007, *ApJ*, 665, 265
 Fernandez, X., Petric, A. O., Schweizer, F., van Gorkom, J. H., 2014, *AJ*, 147, 74
 Fertig, D., Rosenberg, J. L., Patton, D. R., Ellison, S. L., Scudder, J. M., 2015, *MNRAS*, submitted
 Genzel, R., et al. 2010, *MNRAS*, 407, 2091
 Giovanelli, R., et al., 2005a, *AJ*, 130, 2598
 Giovanelli, R., et al., 2005b, *AJ*, 130, 2613
 Giovanelli, R., Haynes, M. P., Herter, T., Vogt, N. P., da Costa, L. N., Freudling, W., Salzer, J. J., Wegner, G., 1997, *AJ*, 113, 53
 Goncalves, T. S., Basu-Zych, A., Overzier, R. A., Perez, L., Martin, D. C., 2014, *MNRAS*, in press
 Guimaraes, R., Petitjean, P., de Carvalho, R. R., Djorgovski, S. G., Noterdaeme, P., Castro, S., Poppe, P. C. Da R., Aghaee, A., 2009, *A&A*, 508, 133
 Haynes, M. P., Giovanelli, R., Chincarini, G. L., 1984, *ARA&A*, 22, 445
 Haynes, M. P., et al., 2011, *AJ*, 142, 170
 Heckman, T. M., et al., 2005, *ApJ*, 619, L5
 Hess, K. M., Wilcots, E. M., 2013, *AJ*, 146, 124
 Hibbard, J. E., van Gorkom, J. H., 1996, *AJ*, 111, 655
 Hibbard, J. E., & Yun, M. S., 1999, *AJ*, 118, 162
 Holwerda, B. W., Pirzkal, N., Cox, T. J., de Blok, W. J. G., Weniger, J., Bouchard, A., Blyth, S.-L., van der Heyden, K. J., 2011, *MNRAS*, 416, 2426
 Hoopes, C. G., et al. 2007, *ApJS*, 2007, *ApJS*, 173, 441
 Hopkins, P. F., et al., 2009, *MNRAS*, 397, 802
 Hopkins, A. M., & Beacom, J. F., 2006, *ApJ*, 651, 142
 Huchtmeier, W. K., Petrosian, A., Gopal-Krishna, McLean, B., Kunth, D., 2008, *A&A*, 492, 367
 Ji, L., Peirani, S., & Yi, S. K., 2014, *A&A*, in press
 Jogee, S., et al., 2009, *ApJ*, 697, 1971
 Kampczyk, P., et al., 2013, *ApJ*, 762, 43
 Kartaltepe J. S., et al., 2010, *ApJ*, 721, 98
 Kaviraj, S., 2014, *MNRAS*, 440, 2944
 Kaviraj, S., et al., 2012, *MNRAS*, 423, 49
 Kauffmann, G., et al., 2003, *MNRAS*, 341, 33
 Keres, D., Katz, N., Weinberg, D. H., Dave, R., 2005, *MNRAS*, 363, 2
 Kilborn, V. A., Forbes, D. A., Barnes, D. G., Koribalski, B. S., Brough, S., Kern, K., 2009, *MNRAS*, 400, 1962
 Koribalski, B., Dickey, J. M., 2004, *MNRAS*, 348, 1255
 L'Huillier, B., Combes, F., & Semelin, B., 2012, *A&A*, 544, 68
 Lackner, C. N., et al., 2014, *ApJ*, submitted
 Lara-Lopez, M. A., Cepa, J., Bongiovanni, A., Perez Garcia, A. M., Ederoclite, A., Castaneda, H., Fernandez Lorenzo, M., Povic, M., Sanchez-Portal, M., 2010, *A&A*, 521, L53
 Lee, C., Chung, A., Yun, M. S., Cybulski, R., Narayanan, G., Erickson, N., 2014, *MNRAS* in press
 Lelli, F., Verheijen, M., Fraternali, F., 2014, *MNRAS*, in press
 Li, C., Kauffmann, G., Heckman, T. M., Jing, Y. P., White, S. D. M., 2008, *MNRAS*, 385, 1903
 Lilly, S. J., Le Fevre, O., Hammer, F., Crampton, D., 1996, *ApJ*, 460, L1
 Lin, L., et al. 2007, *ApJ*, 660, L51
 Lintott, C. J., et al., 2008, *MNRAS*, 389, 1179
 Lotz, J. M., Jonsson, P., Cox, T. J., Primack, J. R., 2008, *MNRAS*, 391, 1137
 Lotz, J. M., Jonsson, P., Cox, T. J., Primack, J. R., 2010a, *MNRAS*, 404, 590
 Lotz, J. M., Jonsson, P., Cox, T. J., Primack, J. R., 2010b, *MNRAS*, 404, 575
 Madau, P., Pozzetti, L., Dickinson, M. E., 1998, *ApJ*, 498, 106
 Mannucci, F., Cresci, G., Maiolino, R., Marconi, A., Gnerucci, A., 2010, *MNRAS*, 408, 2115
 Marasco, A., Fraternali, F., Binney, J. J., 2012, *MNRAS*, 419, 1107
 Marinacci, F., Binney, J., Fraternali, F., Nipoti, C., Ciotti, L., Londrillo, P., 2010, *MNRAS*, 404, 1464
 Mendel, J. T., Palmer, M. J. D., Simard, L., Ellison, S. L., Patton, D. R., 2014, *ApJS*, 210, 3
 Mihos, C., & Hernquist, L., 1996, *ApJ*, 464, 641
 Montuori, M., Di Matteo, P., Lehnert, M. D., Combes, F., Semelin, B., 2010, *A&A*, 518, 56
 Moran, S. M., et al., 2012, *ApJ*, 745, 66
 Moreno, J., Torrey, P., Ellison, S. L., Patton, D. R., Bluck, A. F. L., Bansal, G., Hernquist, L., *MNRAS*, submitted
 Moster, B. P., Maccio, A. V., Somerville, R. S., Naab, T., Cox, T. J. 2011, *MNRAS*, 415, 3750
 Nair, P. B., & Abraham, R. G., 2010, *ApJS*, 186, 427
 Nikolic, B., Cullen, H., Alexander, P., 2004, *MNRAS*, 355, 874
 Noterdaeme, P., et al., 2012, *A&A*, 547, L1
 Oosterloo, T., Fraternali, F., Sancisi, R., 2007a, *AJ*, 134, 1019
 Oosterloo, T. A., Morganti, R., Sadler, E. M., van der Hulst, T., Serra, P., 2007b, *A&A*, 465, 787
 Overzier, R. A., 2011, *ApJ*, 726, L70
 Patton, D. R., Ellison, S. L., Simard, L., McConnachie, A. W., Mendel, J. T., 2011, *MNRAS*, 412, 591
 Patton, D. R., Torrey, P., Ellison, S. L., Mendel, J. T., Scudder, J. M., 2013, *MNRAS*, 433, L59
 Putnam, M. E., Peek, J. E. G., Jounge, M. R., 2012, *ARA&A*, 50, 491
 Rafieferantsoa, M., Dave, R., Angles-Alcazar, D., Katz, N.,

- Kollmeier, J. A., Oppenheimer, B. D., 2014, MNRAS, submitted
- Renaud, F., Bournaud, F., Kraljic, K., Duc, P.-A., 2014, MNRAS, 442, L33
- Robaina, A., et al., 2009, ApJ, 704, 324
- Robertson, B., Cox, T. J., Hernquist, L., Franx, M., Hopkins, P. F., Martini, P., Springel, V., 2006, ApJ, 641, 21
- Sanchez Almeida, J., Elmegreen, B. G., Munoz-Tunon, C., Elmegreen, D. M., 2014, A&AR, in press
- Sancisi, R., Fraternali, F., Oosterloo, T., van der Hulst, T., 2008, A&ARv, 15, 189
- Saintonge, A., 2007, AJ, 133, 2087
- Saintonge, A., 2011, MNRAS, 415, 32
- Saintonge, A., et al., 2012, ApJ, 758, 73
- Sargent, M. T., Daddi, E., Bethermin, M., Aussel, H., Magdis, G., Hwang, H. S., Juneau, S., Elbaz, D., da Cunha, E., 2014, ApJ, submitted
- Satyapal, S., Ellison, S. L., McAlpine, W., Hickox, R. C., Patton, D. R., Mendel, J. T., 2014, MNRAS, in press
- Scott, C., & Kaviraj, S., 2014, MNRAS, 437, 2137
- Scudder, J. M., Ellison, S. L., Torrey, P., Patton, D. R., Mendel, J. T., 2012, MNRAS, 426, 549
- Shabala, S. S., et al., 2012, MNRAS, 423, 59
- Simard, L., Willmer, C. N. A., Vogt, N. P., Sarajedini, V. L., Phillips, A. C., Weiner, B. J., Koo, D. C., Im, M., Illingworth, G. D., Faber, S. M., 2002, ApJS, 142, 1
- Simard, L., Mendel, J. T., Patton, D. R., Ellison S. L., McConnachie, A. W., 2011, ApJS, 196, 11
- Solanes, J. M., Manrique, A., Garcia-Gomez, C., Gonzalez-Casado, G., Giovanelli, R., Haynes, M. P., 2001, ApJ, 548, 97
- Stark, D. V., Kannappan, S. J., Wei, L. H., Baker, A. J., Leroy, A. K., Eckert, K. D., Vogel, S. N., 2013, ApJ, 769, 82
- Thom, C. et al., 2012, ApJ, 758, L41
- Tonnesen, S., & Cen, R., 2012, MNRAS, 425, 2313
- Torrey, P., Cox, T. J., Kewley, L. J., Hernquist, L., 2012, ApJ, 746, 108
- Ueda, J., et al. 2014, ApJS, 214, 1
- Wang, J., et al., 2011, MNRAS, 413, 1373
- Wang, W.-H., Lo, K. Y., Gao, Y., Gruendl, R. A., 2001, AJ, 122, 140
- Wang, J. L., Xia, X. Y., Mao, S., Cao, C., Wu, Hong, Deng, Z. G., 2006, ApJ, 649, 722
- Wong, K. C., et al., 2011, ApJ, 728, 119
- Woods, D. F., Geller, M. J., Barton, E. J., 2006, AJ, 132, 197
- Xu, C. K., et al., 2012, ApJ, 760, 72
- Yun, M. S., & Hibbard, J. E., 2001, ApJ, 550, 104
- Zabludoff, A. I., Zaritsky, D., Lin, H., Tucker, D., Hashimoto, Y., Shectman, S. A., Oemler, A., Kirshner, R. P., 1996, ApJ, 466, 104
- Zafar, T., Peroux, C., Popping, A., Milliard, B., Deharveng, J.-M., Frank, S.
- Zwaan, M. A., Kuntschner, H., Pracy, M. B., Couch, W. J., 2013, MNRAS, 432, 492